Electronic Supplementary Material (ESI)

for

EHDTA†: a green approach to efficient Ln^{3+}-chelators

Fabio Travagin,[a] Maria Ludovica Macchia,[b] Toni Grell,[c] Judit Bodnár,[d]
Zsolt Baranyai,[e*] Flavia Artizzu,[f] Mauro Botta[b*] and Giovanni B. Giovenzana[a*]

[a] Dipartimento di Scienze del Farmaco, Università del Piemonte Orientale, Largo Donegani 2/3, 28100 Novara, Italy. E-mail: giovannibattista.giovenzana@uniupo.it
[b] Dipartimento di Scienze e Innovazione Tecnologica, Università del Piemonte Orientale, Via T. Michel 11, 15121 Alessandria, Italy. E-mail: mauro.botta@uniupo.it
[c] Dipartimento di Chimica, Università degli Studi di Milano, Via Golgi 19, 20133 Milano, Italy
[d] Department of Inorganic and Analytical Chemistry, University of Debrecen, H-4010, Debrecen, Egyetem tér 1., Hungary
[e] Bracco Imaging SpA, CRB Trieste, AREA Science Park, ed. Q – S.S. 14 Km 163,5 – 34149 Basovizza (TS) Italy. E-mail: zsolt.baranyai@bracco.com
[f] Dipartimento per lo Sviluppo Sostenibile e la Transizione Ecologica, P.zza S. Eusebio 5, 13100 Vercelli, Italy

Table of contents

† EHDTA = 2,5-Epoxyhexane-1,6-diamine-*N*,*N*,*N'*,*N'*-tetraacetic acid

NMR spectra

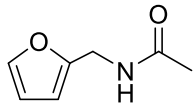

2

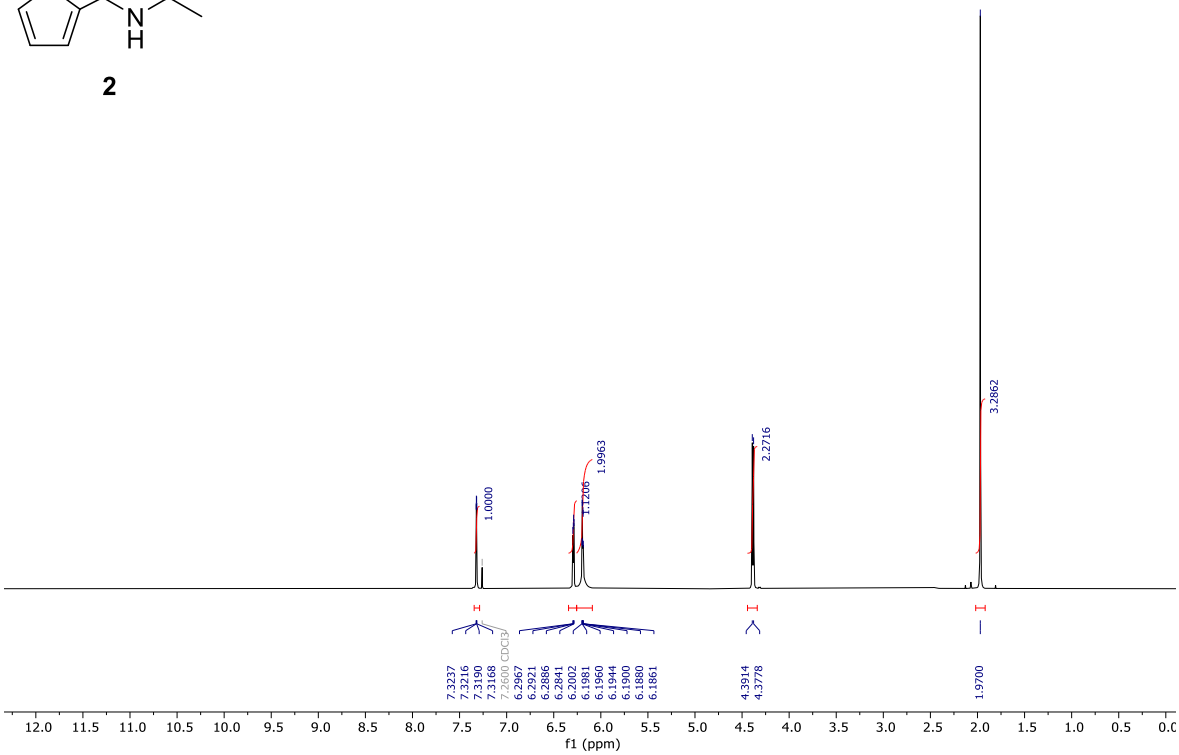

Figure S1. ^{1}H NMR spectrum of compound **2**.

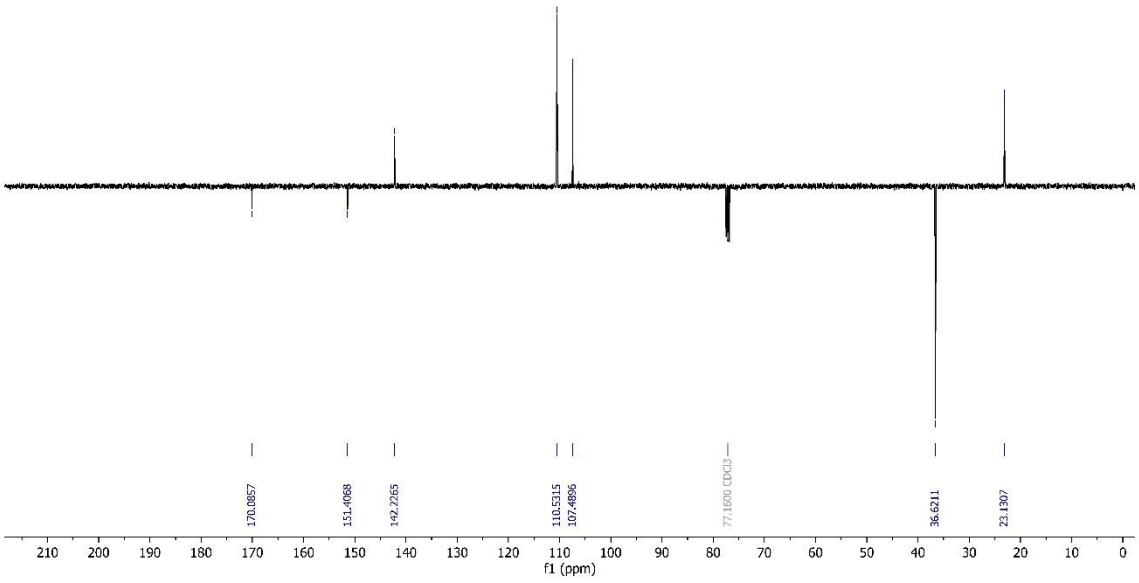

Figure S2. ^{13}C APT NMR spectrum of compound **2**.

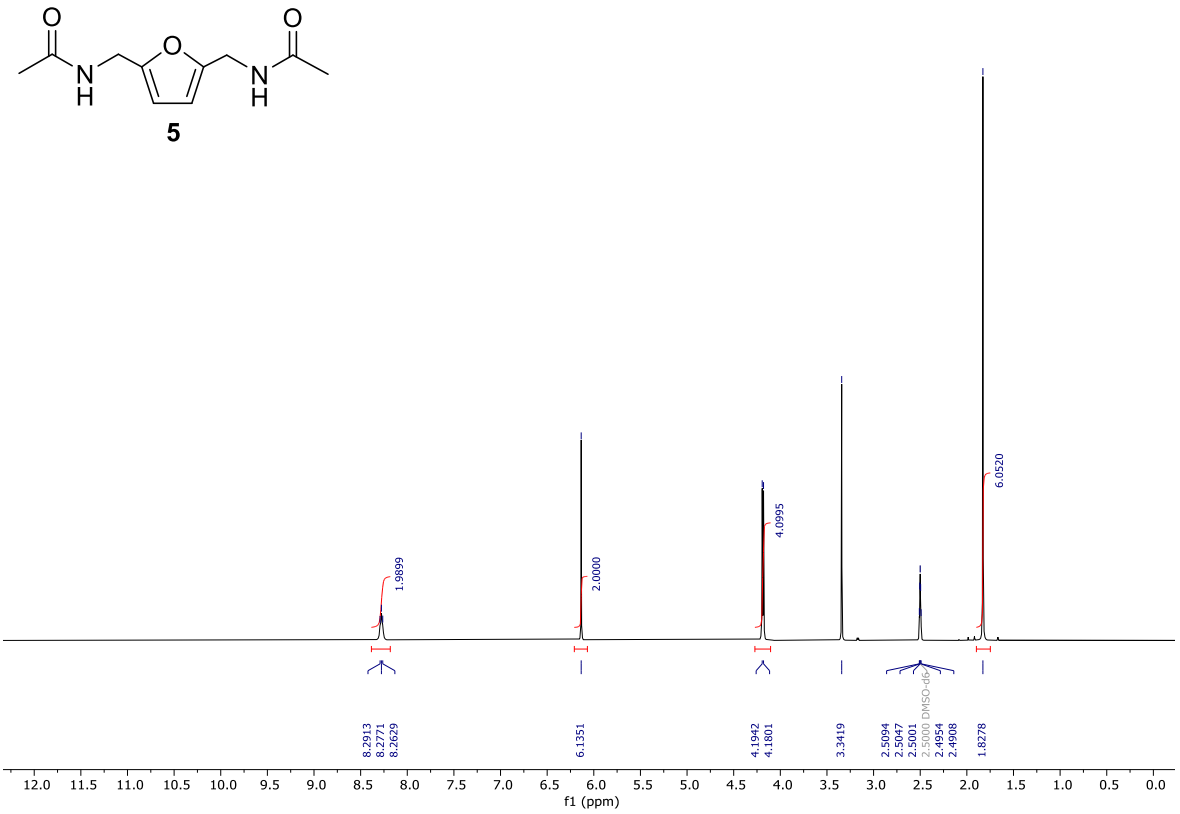

Figure S3. ^{1}H NMR spectrum of compound **5**.

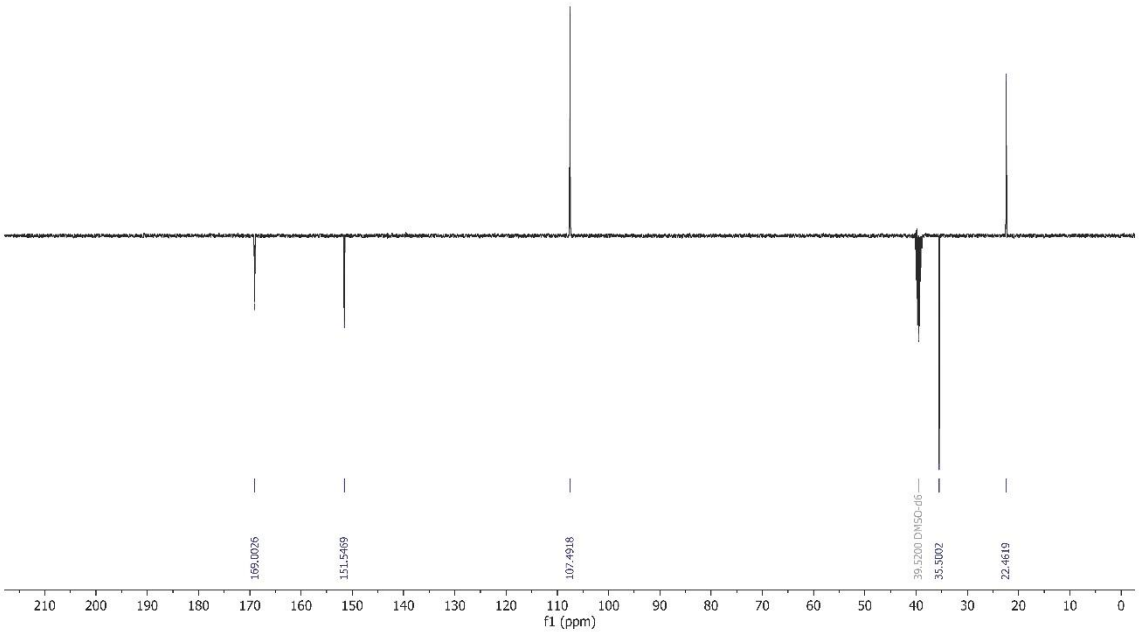

Figure S4. ^{13}C APT NMR spectrum of compound **5**.

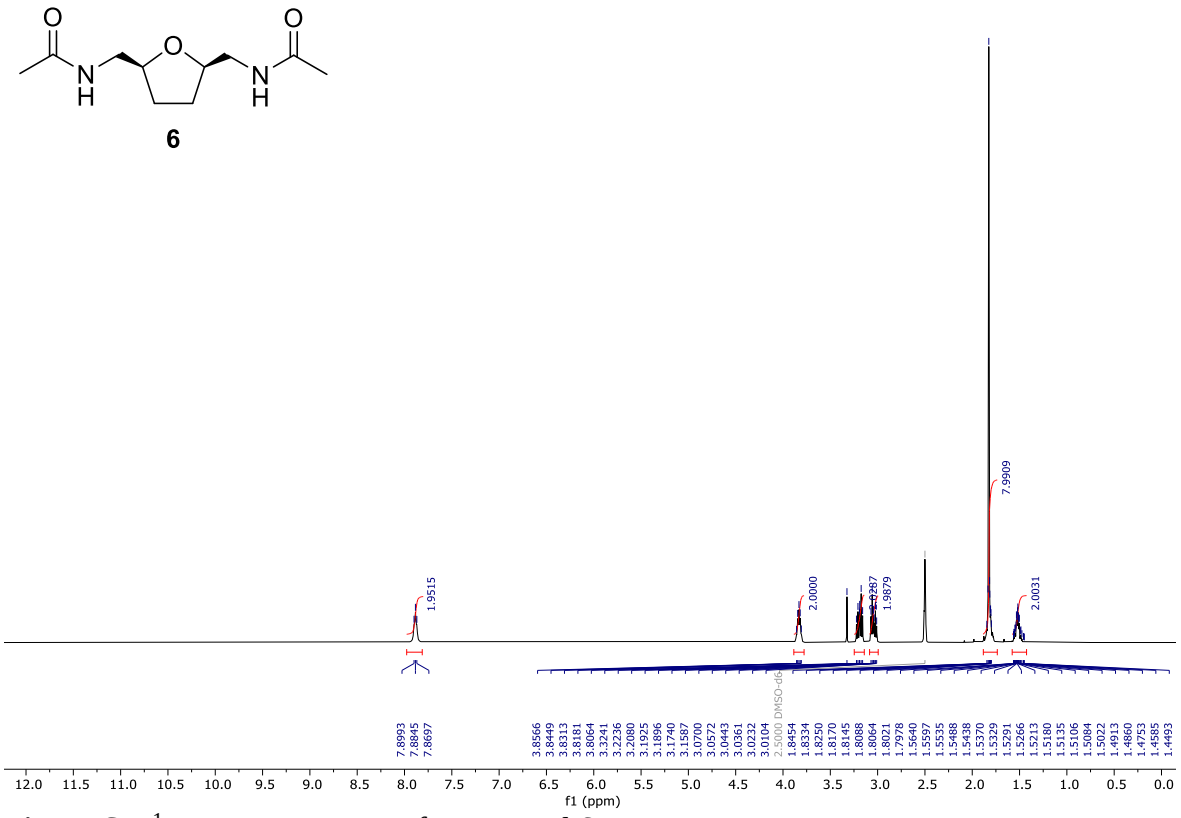

Figure S5. ^{1}H NMR spectrum of compound **6**.

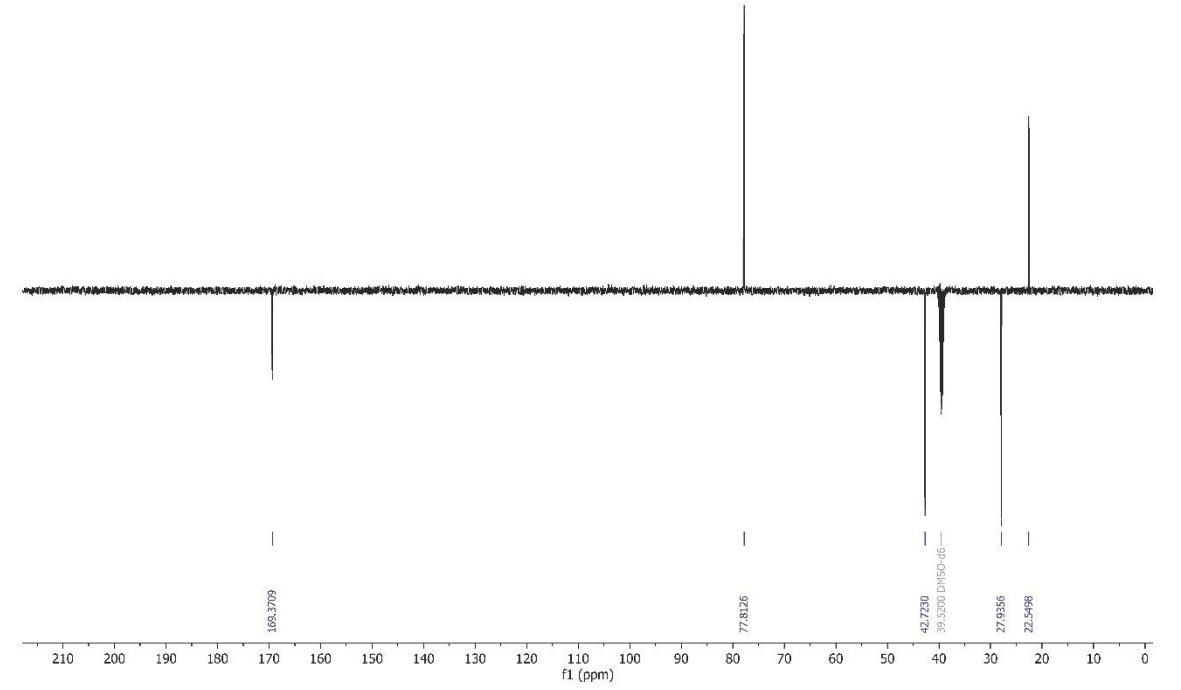

Figure S6. ^{13}C APT NMR spectrum of compound **6**.

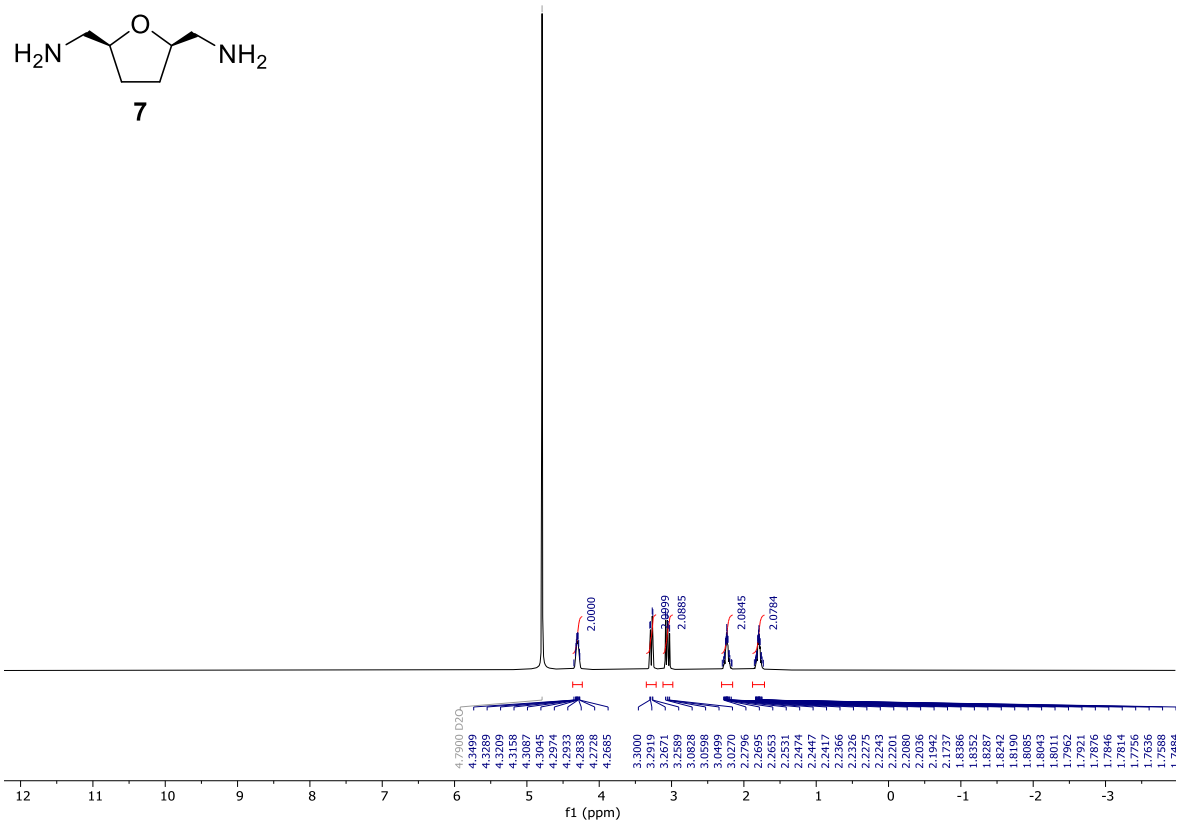

Figure S7. ^{1}H NMR spectrum of compound **7**.

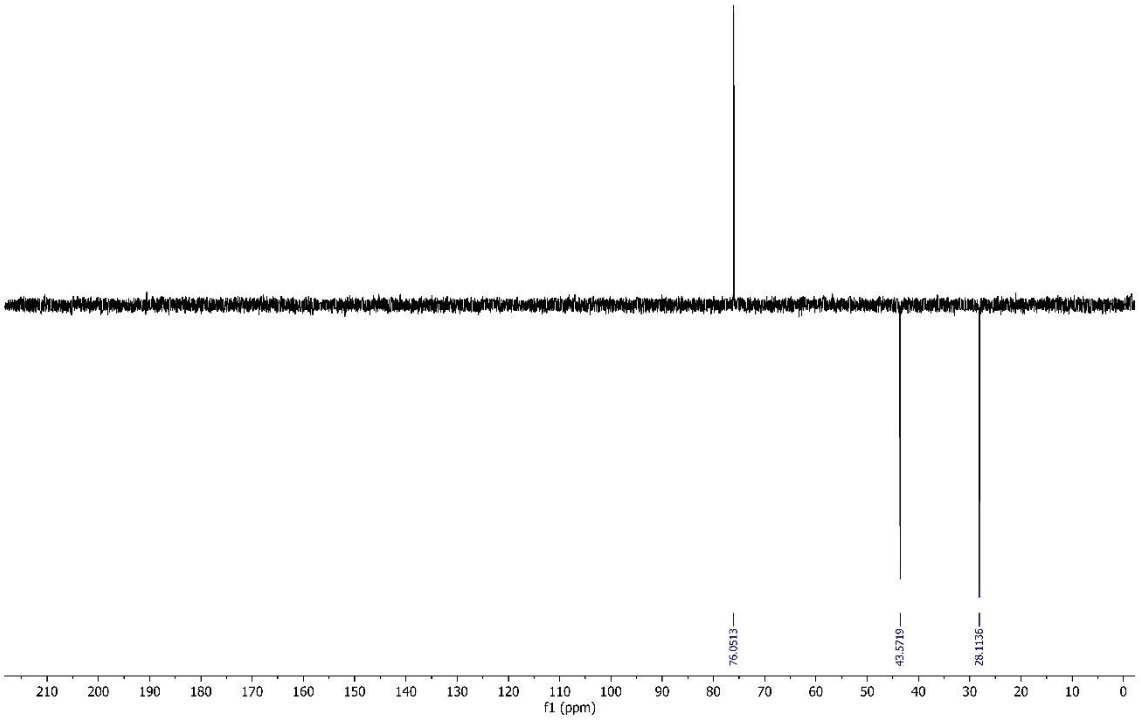

Figure S8. ^{13}C APT NMR spectrum of compound **7**.

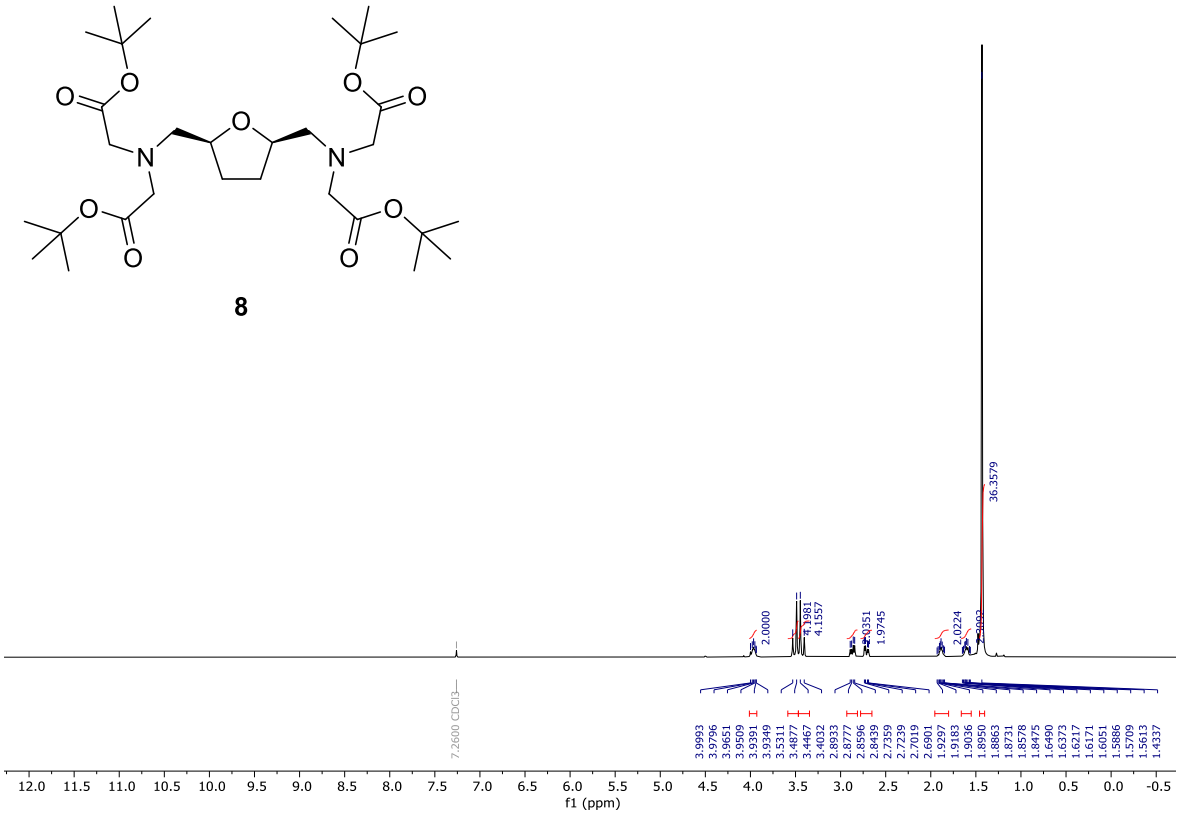

Figure S9. ^{1}H NMR spectrum of compound **8**.

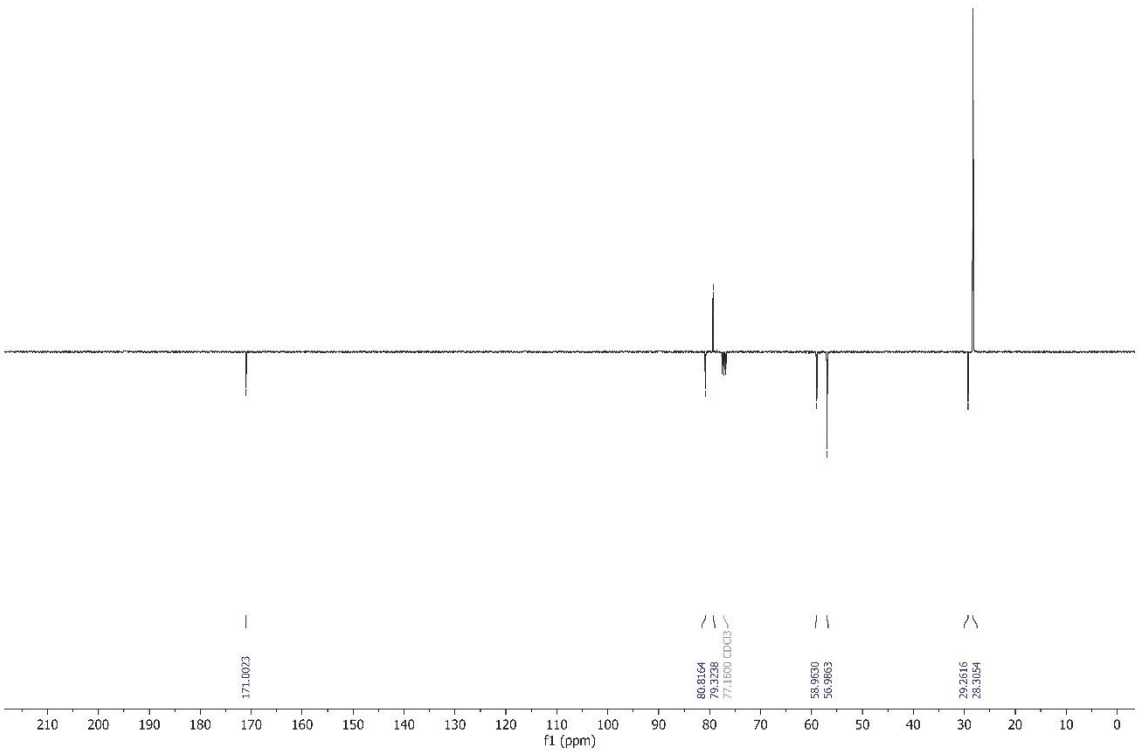

Figure S10. ^{13}C APT NMR spectrum of compound **8**.

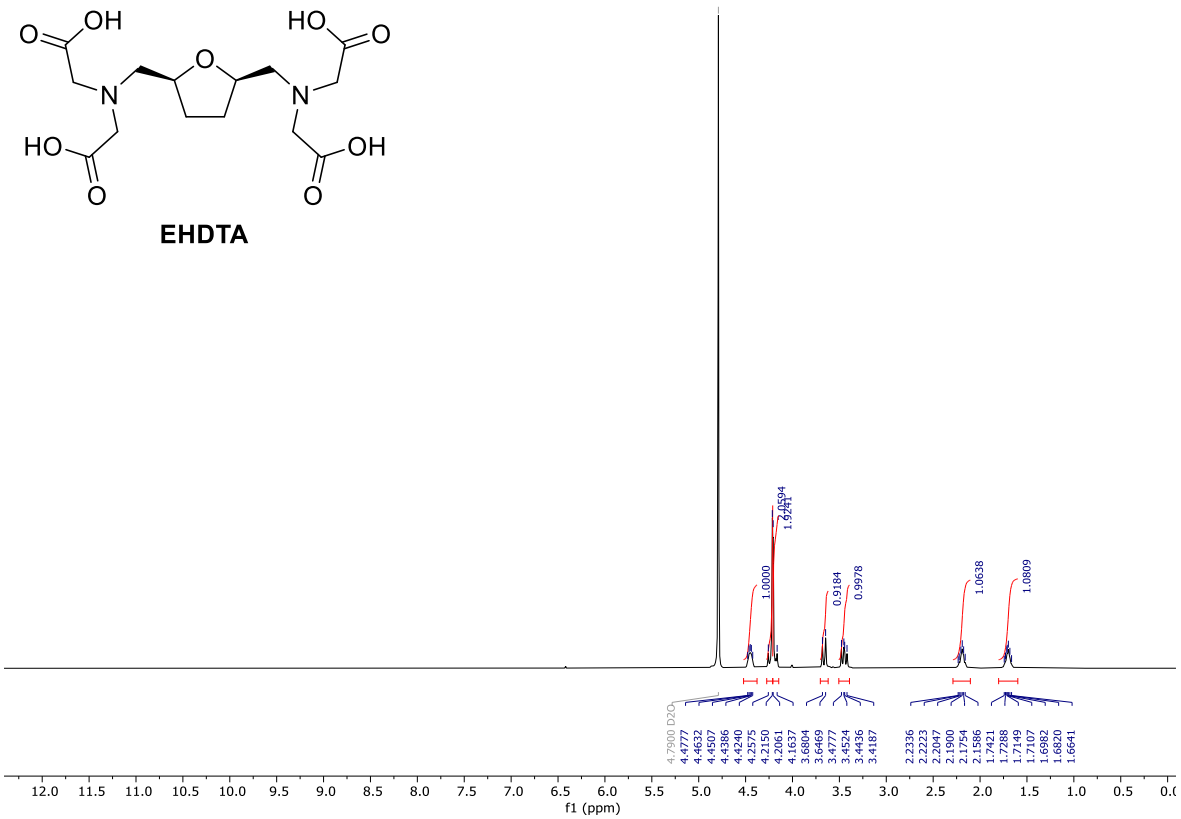

Figure S11. ^{1}H NMR spectrum of **EHDTA**.

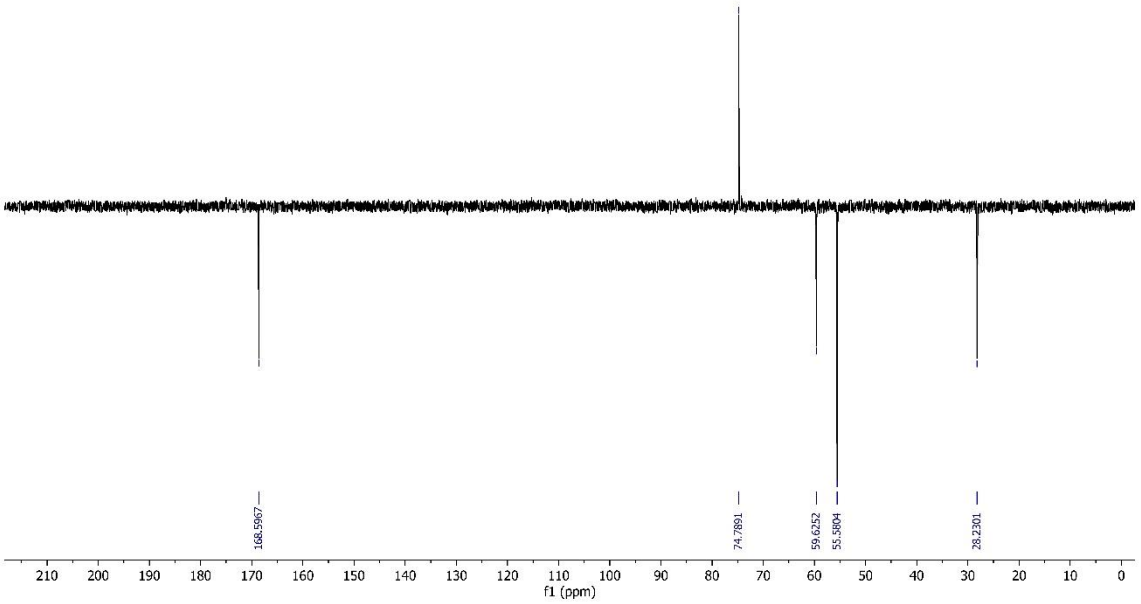

Figure S12. ^{13}C APT NMR spectrum of **EHDTA**.

HRMS spectra

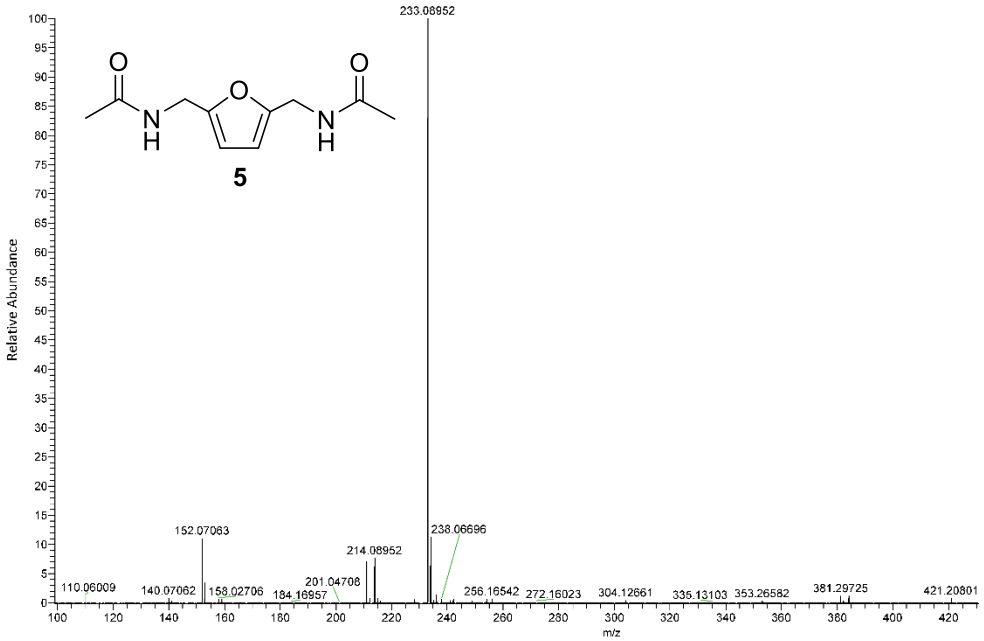

Figure S13. HRMS spectrum of compound **5**.

Figure S14. HRMS spectrum of compound **6**.

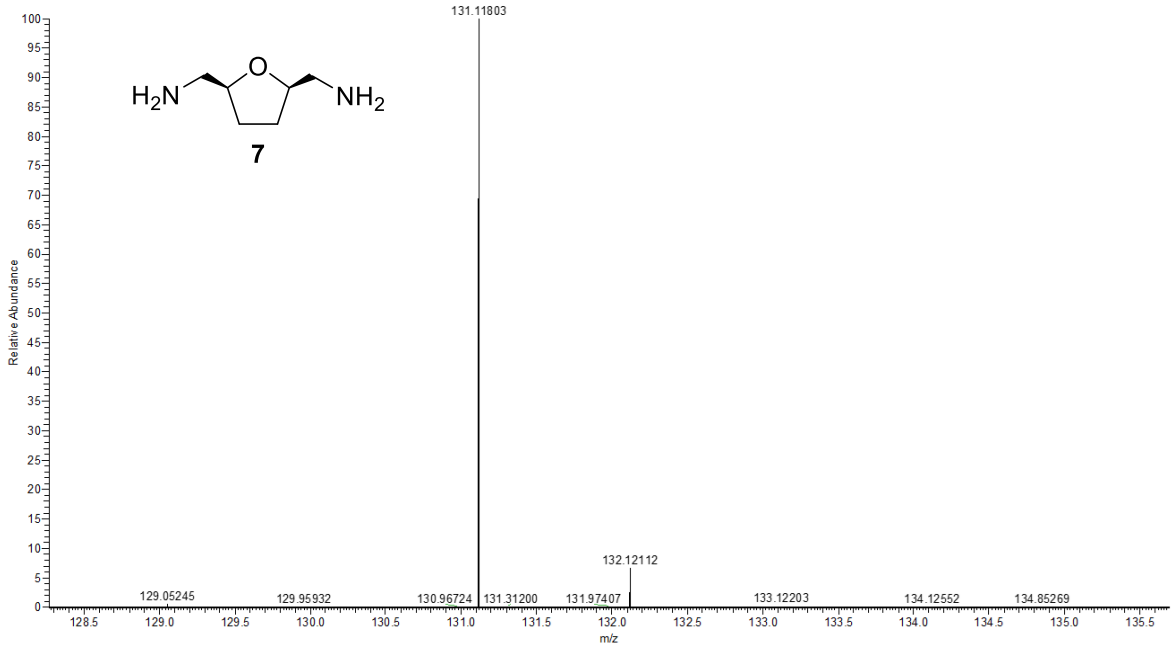

Figure S15. HRMS spectrum of compound **7**.

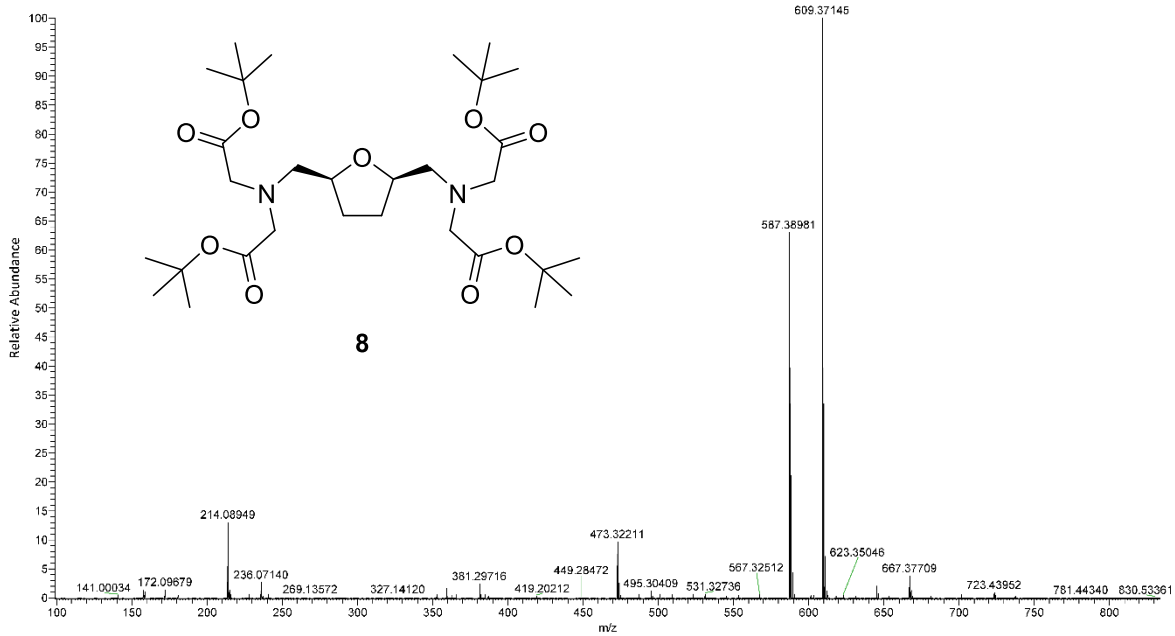

Figure S16. HRMS spectrum of compound **8**.

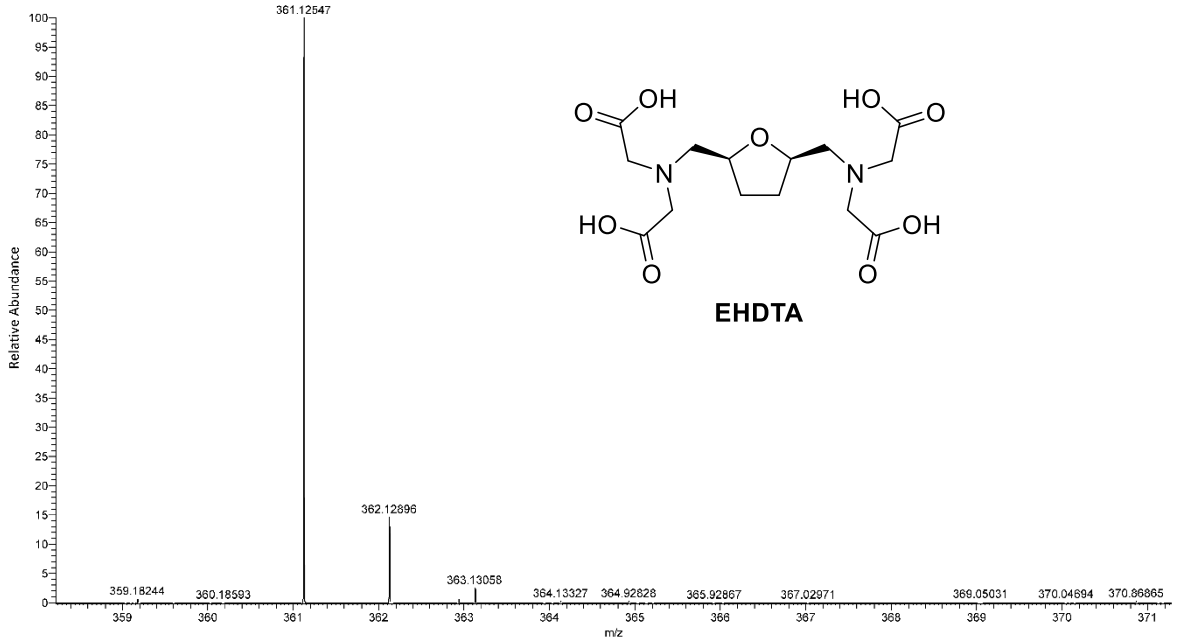

Figure S17. HRMS spectrum of **EHDTA**.

Protonation and complexation properties of EHDTA ligand

The protonation constants of the EHDTA ligand, defined by Eq. (S1), have been determined by pH-potentiometry and the logK_i^H values are listed in Table S1. (standard deviations are shown in parentheses).

$$K_i^H = \frac{[H_iL]}{[H_{i-1}L][H^+]} \qquad (S1)$$

where i=1, 2…5. The protonation constants were also determined with the use of the pH-dependent ^{1}H NMR chemical shifts of the non-labile protons of the EHDTA. The chemical shift (δ_H) of the ^{1}H-NMR signals obtained at different pH values indicates the protonation/deprotonation of the different donor atoms in the EHDTA (Figure S18). Since the protonation/deprotonation of the donor atoms is fast process on the NMR time scale, the chemical shifts of the observed signals represent a weighted average of the shifts of the different species involved in a specific protonation step (Eq. (S2)).[1]

$$\boldsymbol{\delta_{H(obs)} = \sum x_i \delta_H^{H_iL}} \qquad (S2)$$

where, $\delta_{H(obs)}$ is the observed chemical shift of a given signal, x_i and δ_H^{HiL} are the molar fraction and the chemical shift of the involved species, respectively. The observed chemical shifts $\delta_{H(obs)}$ were fitted with Eq. (S2) (the molar fractions x_i of the different protonated species were expressed with the use of the protonation constants K_i^H). The fits of the experimental data points are shown in Figure S18 and the obtained logK_i^H values are listed in Table S1.

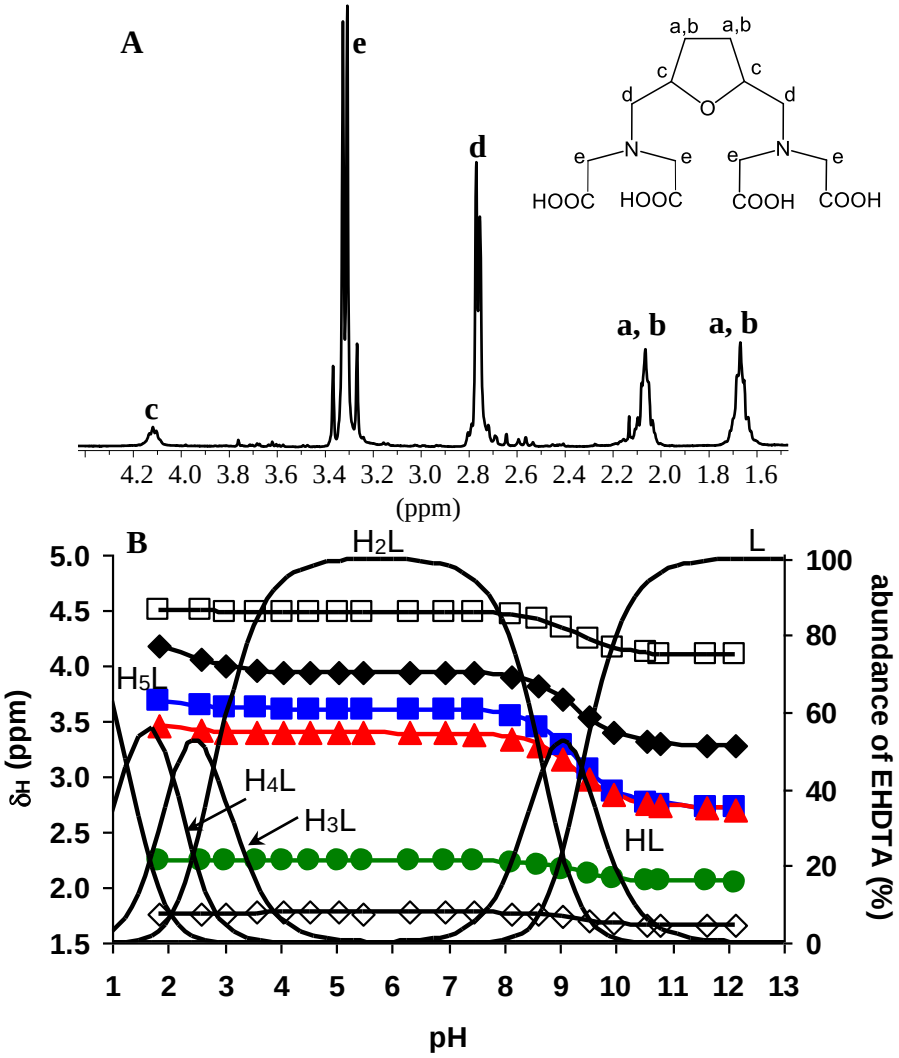

Figure S18. ^{1}H-NMR spectrum of the EHDTA ligand at pH=11.5 (**A**) and ^{1}H-NMR titration curve of the EHDTA (**B**): a, b (◊, •), c (□), d (▲, ■) and e (♦) ([EHDTA]=0.01 M, 400 MHz, 0.1 M KCl, 25°C)

There are 5 multiplets in the ^{1}H-NMR spectra of the EHDTA (Figure S18). Protons of the ring (*a*, *b*, *c*), the side arm (*d*) and acetate groups (*e*) give rise to three resolved multiplets (*a*, *b*, *c*) and two AB systems (*d*, *e*). At pH=11.5, the K^{+} complex is present and the ligand exchange between $K(EHDTA)^{3-}$ and $EHDTA^{4-}$ is presumably fast on the NMR time scale. On the other hand, the structure of $K(EHDTA)^{3+}$ complex is presumably rigid, cease the equivalence of the *d* and *e* methylene protons (AB doublets at 2.8 and 3.3 ppm, respectively). Starting from the deprotonated $EHDTA^{4-}$, the addition of two equivalents acid results in a significant downfield shift of the signals of *c*, *d* and *e* protons indicating that the first and second protonation processes characterized by $\log K_1^{H}$ and $\log K_2^{H}$ take place at the nitrogen

atoms of iminodiacetate groups. Further lowering of pH resulted in the downfield shift of the signals of the methylene protons of the pendant (*d*) and the acetate (*e*) confirming that the $\log K_3^H$ - $\log K_5^H$ values are related to the protonation of the carboxylate groups at pH<4. The $\log K_i^H$ values of the EHDTA obtained by ^{1}H-NMR spectroscopy agree well with the data determined by pH-potentiometry.

Table S1. Protonation constants of the EHDTA, OBETA and TTHA ligands (25°C):

	EHDTA				**OBETA[a,b]**	**TTHA**
I	**0.1 M KCl**		**0.15 M NaCl**	**0.1 M $NaNO_3$ [c]**	**0.1 M KCl**	**0.1 M KCl**
Method	pH-pot.	^{1}H-NMR	pH-pot.	pH-pot.	pH-pot	pH pot
$\log K_1^H$	9.40 (1)	9.35 (2)	8.99 (1)	8.95	9.34	10.53 (1)
$\log K_2^H$	8.70 (1)	8.79 (2)	8.49 (1)	8.67	8.62	9.47 (1)
$\log K_3^H$	2.84 (1)	2.78 (8)	2.83 (1)	2.73	3.19	6.09 (1)
$\log K_4^H$	2.11 (1)	–	1.96 (1)	2.42	2.19	4.05 (1)
$\log K_5^H$	1.30 (1)	–	1.44 (2)	–	1.77	2.83 (1)
$\log K_6^H$	–	–		–	–	2.17 (1)
$\log K_7^H$	–	–		–	–	1.67 (1)
$\Sigma\log K_i^H$	24.35	–	23.71	–	25.11	36,81

[a] Ref. [2]; [b] Ref. [3]; [c] Ref.[4].

The comparison of the $\log K_i^H$ values in Table S1 reveals that the protonation constants of EHDTA is very similar to those of the corresponding $\log K_i^H$ values of OBETA ($\log K_3^H$ value of EHDTA is somewhat lower than that of OBETA). Interestingly, the $\log K_1^H$ and $\log K_2^H$ values of EHDTA obtained in the presence of 0.15 M NaCl are lower by about 0.4 and 0.2 log*K* units than those values determined in 0.1 M KCl solution due to the formation of $Na(EHDTA)^{3-}$ complex. The $\Sigma\log K_i^H$ values, presented in Table S1, indicate that the total basicity of the EHDTA is similar to that of OBETA. By taking into account the similar basicity of the EHDTA and OBETA, the stability constants of the Ln(III) complexes with EHDTA and OBETA are expected to be comparable. However, in determining the stability constants of the Ln(III) complexes, the preorganization of the coordinating donor atoms play an important role. In order to investigate the effect of the rigid five membered ring on the thermodynamic properties of the metal complexes, the stability constants of Ln(III)-, Mg(II)-Ca(II)-, Sr(II)-, Zn(II)- and Cu(II)-complexes with EHDTA have been determined and compared with the corresponding complexes formed with OBETA.

The stability and protonation constants of the metal complexes formed with the EHDTA ligand are defined by Eqs. (S3) and (S4):

$$K_{\mathrm{ML}} = \frac{[\mathrm{ML}]}{[\mathrm{M}][\mathrm{L}]} \qquad (S3)$$

$$K_{\mathrm{MH_iL}} = \frac{[\mathrm{MH_iL}]}{[\mathrm{MH_{i-1}L}][\mathrm{H^+}]} \qquad i=1,2 \qquad (S4)$$

The stability and protonation and stability constants of the EHDTA complexes have been calculated from the titration curves obtained at 1:1 metal to ligand concentration ratio. The best fitting was obtained by using the model which includes the formation of *ML*, *MHL* and MH_2L species in equilibrium. The titration data of the H_4EHDTA ligand in the presence Cu^{2+} indicate base consuming processes at pH>9. These processes can be interpreted by assuming the coordination of OH^- ion to the metal ion according to Eq. (S5).

$$K_{\mathrm{MLH_{-1}}} = \frac{[\mathrm{ML}]}{[\mathrm{MLH_{-1}}][\mathrm{H^+}]} \qquad (S5)$$

pH-potentiometric titrations were also made at 2:1 metal-to-ligand ratio in order to examine the possible formation of dinuclear complexes in the Zn^{2+}-EHDTA and Cu^{2+}-EHDTA systems as it was found in the Zn^{2+}-OBETA and Cu^{2+}-OBETA systems. The stability and protonation constants of the dinuclear M_2L and ternary hydroxo complexes $[M_2(L)(OH)_m]$ (m = 1, 2) are defined by Eqs. (S6)-(S8):

$$K_{M_2L} = \frac{[M_2L]}{[ML][M]} \qquad (S6)$$

$$K_{M_2LH_{-1}} = \frac{[M_2L]}{[M_2(L)H_{-1}][H^+]} \qquad (S7)$$

$$K_{M_2LH_{-2}} = \frac{[M_2(L)H_{-1}]}{[M_2(L)H_{-2}][H^+]} \qquad (S8)$$

The stability constants obtained by pH-potentiometric titration are presented and compared with those of OBETA in Tables S2 and S3. The stability constants of Mg(II)-, Ca(II)- and Sr(II)-complexes of EHDTA and OBETA ligands are very similar. logK_{ML} values increase from Mg(II)- to Ca(II)- and decreases for Sr(II)-complexes, which highlights the metal ion size selectivity of both heptadentate ligands (Mg(II)-ion is too small, whereas the Sr(II)-ion is too large for the cavity of EHDTA and OBETA ligands).

Table S2. Stability and protonation constants of Mg(II)-, Ca(II)-, Sr(II)- and Ln(III)-complexes formed with EHDTA, OBETA and DTPA ligands (25°C)

	EHDTA	**OBETA[a,b]**	**DTPA[c,d]**
Ionic strength	**0.1 M KCl**		**0.1 M KNO_3**
MgL	**7.89 (1)**	**7.95 (2)**	**9.27**
MgHL	5.74 (3)	–	6.9
CaL	**10.27 (1)**	**9.77 (3)**	**10.75**
CaHL	4.64 (3)	–	6.4
SrL	**9.06 (1)**	**–**	**9.79**
SrHL	5.29 (3)	–	5.4
LaL	**17.12 (2)**	**16.89**	**19.48**
LaHL	2.33 (3)	2.85	–
CeL	**17.84 (2)**	**17.34**	**20.50**
CeHL	1.93 (5)	2.53	–
NdL	**18.65 (2)**	**18.39**	**21.60**
NdHL	1.89 (4)	2.37	–
SmL	**–**	**19.02**	**22.34**
SmHL	–	2.22	–
EuL	**19.59 (1)**	**19.13**	**22.39**
EuHL	1.88 (3)	2.21	–
GdL	**19.62 (3)**	**19.37**	**22.46**
GdHL	2.06 (6)	2.20	–
DyL	**19.56 (2)**	**18.87**	**22.82**
DyHL	1.97 (5)	2.28	–
HoL	**–**	**18.93**	**22.78**
HoHL	–	2.29	–
ErL	**19.46 (2)**	**18.46**	**22.74**
ErHL	1.95 (5)	2.23	–
YbL	**19.44 (2)**	**18.31**	**22.62**
YbHL	1.83 (4)	2.30	–
LuL	**19.36 (2)**	**17.93**	**22.44**
LuHL	1.88 (5)	2.42	–

[a] Ref. [2]; [b] Ref. [3]; [c] Ref. [5]; [d] Ref. [6]

Table S3. Stability and protonation constants of Zn(II)- and Cu(III)-complexes formed with EHDTA, OBETA and DTPA ligands (25°C)

	EHDTA		**OBETA**				**DTPA**[c]	
	Cu^{2+}	**Zn^{2+}**	**Cu^{2+}**		**Zn^{2+}**		**Cu^{2+}**	**Zn^{2+}**
	0.1 M KCl	0.1 M KCl	0.1 M KCl [a]	0.1 M KNO_3 [b]	0.1 M KCl [a]	0.1 M KNO_3 [b]	0.15 M NaCl	
ML	**16.37 (3)**	**14.20 (1)**	**18.40**	**18.0**	**15.00**	**15.2**	**23.40**	**17.58**
MHL	4.75 (2)	3.54 (1)	3.71	4.22	3.18	2.75	4.63	5.37
MH_2L	2.07 (2)	–	2.05	–	–	–	2.67	2.38
MLH_{-1}	11.39 (3)	–	–	–	–	–	–	–
M_2L	**5.30 (5)**	**–**	**5.74**	**–**	**2.05**	**–**	**6.56**	**4.33**
M_2LH_{-1}	5.27 (3)	–	6.42	–	–	–	–	–
M_2LH_{-2}	9.41 (3)	–	8.56	–	–	–	–	–

[a] Ref. [3]; [b] Ref. [7]; [c] Ref. [8]

Interestingly, the stability constant of the $Cu(EHDTA)^{2-}$ and $Zn(EHDTA)^{2-}$ complexes are about 2.0 and 0.8 log*K* unit lower than that of Cu(OBETA) and Zn(OBETA) complexes, which might be explained by the unfavourable coordination cage formed by the preorganized donor atoms of the EHDTA ligand. The lower flexibility of the EHDTA is also reduce the affinity of the ligand to the second metal ion, which is clearly reflected by the lack of the Zn_2(EHDTA) and lower stability of the Cu_2(EDTA) complex.

Finally, the Mg(II)-, Ca(II)-, Sr(II)-, Zn(II)-, Cu(II)- and Ln(III)- complexes with both EHDTA and OBETA can be protonated at low pH values, and their protonation constants were determined by pH potentiometry (Tables S2 and S3). Similarly to the $Zn(OBETA)^{2-}$ and $Cu(OBETA)^{2-}$, the Zn(II)- and Cu(II)-complexes of EHDTA likely embody one or two non- or weakly coordinated donor atoms (presumably carboxylate-O), which can be protonated at pH values around 3−4. On the other hand, in both $Ln(EHDTA)^-$ and $Ln(OBETA)^-$ complexes all the carboxylate groups are strongly coordinated to the Ln(III)-ion and thus their protonation might occur at more acidic pH ($\log K_{LnHL}$ = 1.8−2.3).

Kinetic inertness of the $Gd(EHDTA)^-$

Transmetallation of the $Gd(EHDTA)^-$ with Cu^{2+} and Eu^{3+} ions.

The kinetic inertness of metal-complexes is generally characterized either by the rates of their dissociation measured in 0.1 M HCl or by the rates of transmetallation reaction, with Zn^{2+} and Cu^{2+} or Eu^{3+}.[2,9–11] For a direct comparison of the kinetic properties of $Gd(EHDTA)^-$ and $Gd(OBETA)^-$, the same method and identical conditions were used as it was applied in

the case of $Gd(OBETA)^{-}$.[2] The rates of the transmetallation reactions (Eq. (S9)) were studied by spectrophotometry with the use of Cu^{2+} and Eu^{3+} as exchanging metal ions:

$$GdL + M^{n+} \rightleftharpoons ML + Gd^{3+} \qquad (S9)$$

where $M^{n+} = Cu^{2+}$ or Eu^{3+}. In the presence of 10 – 40 fold excess of the exchanging ion the transmetallation can be treated as a pseudo-first-order process and the rate of reactions can be expressed with the Eq. (S10), where k_d is a pseudo-first-order rate constant and $[GdL]_t$ is the total concentration of the Gd(III)-complex.

$$-\frac{d[GdL]_t}{dt} = k_d[GdL]_t \qquad (S10)$$

The rates of the transmetallation reactions have been studied at different concentrations of the exchanging ions in the pH range 3.5 – 6.0. The obtained rate constants k_d are presented in Figures S19 and S20 as a function of pH and $[H^+]$.

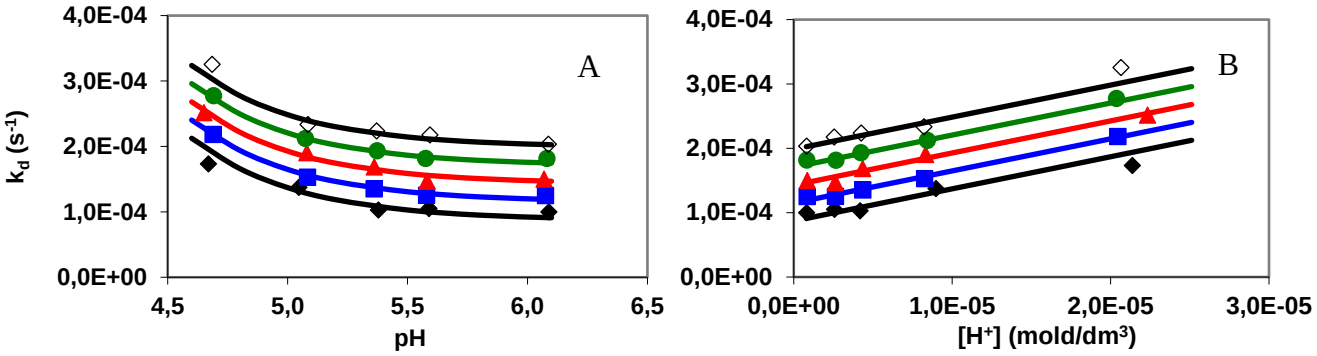

Figure S19. The rate constants (k_d) for the transmetallation reaction of $Gd(EHDTA)^{-}$ with Eu^{3+} as a function of pH (**A**) and $[H^+]$ (**B**) ([GdL]=1.0 mM, $[Eu^{3+}]$=10 (♦), 20 (■), 30 (▲), 40 (●) and 50 mM (◊)**,** pH=4.7, 5.0, 5.4, 5.7 and 6.0, 0.1 M KCl, 25°C)

As it can be seen in Figures S19 and S20 the k_d values increase with increase of the $[H^+]$, (particularly at lower $[Cu^{2+}]$ or $[Eu^{3+}]$) and also with increasing $[Cu^{2+}]$ or $[Eu^{3+}]$ at pH > 4.0. The increase in the k_d values with increasing H^+ concentration can be interpreted in terms of the relatively slow proton assisted dissociation of $Gd(EDHTA)^{-}$, followed by a fast reaction between the free ligand and the exchanging metal ions Cu^{2+} or Eu^{3+}. The dependence of k_d on the $[H^+]$ can be expressed as a first-order function of $[H^+]$ which indicates that the exchange can take place by proton-independent (Eq. (S11)) and proton assisted (Eqs. (S12) and (S13)) pathways. The proton assisted dissociation of $Gd(EHDTA)^{-}$ can be explained by the equilibrium formation of a protonated Gd(HEHDTA) complex, which dissociates spontaneous (Eq. (S12) and proton assisted (Eq. (S13)) mechanisms.

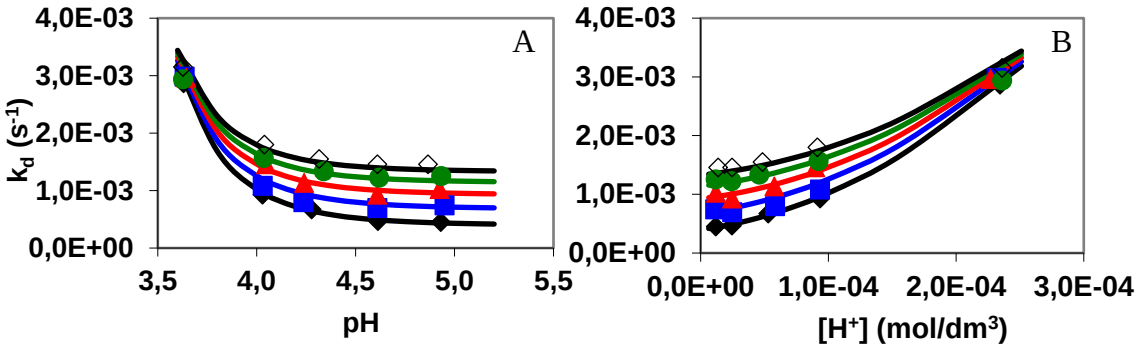

Figure S20. The rate constants (k_d) for the transmetallation reaction of $Gd(EHDTA)^-$ with Cu^{2+} as a function of pH (**A**) and $[H^+]$ (**B**) ([GdL]=0.1 mM, $[Cu^{2+}]$=1.0 (♦), 2.0 (■), 3.0 (▲), 4.0 (●) and 5.0 mM (◊)**,** pH=3.6, 4.0, 4.3, 4.6 and 5.0, [NMP]=[DMP]=0.01 M, 0.1 M KCl, 25°C)

$$GdL \xrightarrow{k_0} Gd^{3+} + H_xL \qquad (S11)$$

$$Gd(HL) \xrightarrow{k_{GdHL}} Gd^{3+} + H_xL \qquad (S12)$$

$$Gd(HL) + H^+ \xrightarrow{k^H_{GdHL}} Gd^{3+} + H_xL \qquad (S13)$$

The increase in the rate of the exchange reactions with increasing $[Cu^{2+}]$ or $[Eu^{3+}]$ indicates that the reaction can take place with the direct attack of the exchanging metal ion on the Gd(III)-complex, via the formation of hetero-dinuclear intermediate. In the case of the $Gd(OBETA)^-$ and $Ln(DTPA)^{2-}$ complexes the formation of homo- and hetero-dinuclear complexes was detected by spectrophotometry and by ^{1}H-NMR spectroscopy.[2,11] The formation of the hetero-dinuclear $[Gd(EHDTA)M]^+$ complex can be expressed by Eq. (S14).

$$GdL + M^{n+} \overset{K^*_{GdLM}}{\rightleftharpoons} [Gd(L)M]$$

$$K^*_{GdLM} = \frac{[Gd(L)M]}{[GdL][M^{n+}]} \qquad (S14)$$

It can be assumed that in the hetero-dinuclear intermediate, the functional groups of the EHDTA ligand are slowly transferred from the Gd^{3+} to the attacking Cu^{2+} or Eu^{3+} step by step.

$$[Gd(L)M] \xrightarrow{k_{GdLM}} Gd^{3+} + ML \qquad (S15)$$

The trend in the k_d values in Figure S20 show that the increase of the concentration of Cu^{2+} results in a slight decrease in the k_d values at higher H^+ concentration. This phenomenon can be interpreted by considering that the concentration of the dinuclear species increases with the increase of the concentration of the exchanging metal ion, when the concentration of the monoprotonated Gd(HEHDTA) decreases, which results in the decrease of the rate of the proton-assisted dissociation of the complex ($[M^{n+}]>>[H^+]$). Similar results were obtained in the exchange reactions of $Gd(OBETA)^-$ and $Ln(DTPA)^{2-}$ complexes.[2,11]

By taking into account all the possible pathways, the rate of the transmetallation of $Gd(EHDTA)^-$ can be expressed by Eq. (S16), where the [GdHL] and [GdLM] are the concentrations of the protonated and the hetero-dinuclear intermediates, respectively:

$$-\frac{[\mathrm{GdL}]_{\mathrm{tot}}}{\mathrm{dt}} = k_0[\mathrm{GdL}] + k_{\mathrm{GdLH}}[\mathrm{GdHL}] + k^{\mathrm{H}}_{\mathrm{GdHL}}[\mathrm{GdHL}] + k_{\mathrm{GdLM}}[\mathrm{Gd(L)M}] \qquad (S16)$$

By taking into account the total concentration of the Gd(III)-complex ([GdL]t=[GdL]+[Gd(HL)]+[Gd(L)M]), the equations defining the protonation constant of the monoprotonated complex (Eq. (S4), the stability constant of the hetero-dinuclear complex (Eq. (S14)) and Eq. (S10), the pseudo-first-order rate constant can be expressed as follows:

$$k_{\mathrm{d}} = \frac{k_0 + k_1[H^+] + k_2[H^+]^2 + k_3[M^{n+}]}{1 + K_{GdHL}[H^+] + K^*_{GdLM}[M^{n+}]} \qquad (S17)$$

The rate constants, k_0, $k_1 = k_{GdHL} \times K_{GdHL}$, $k_2 = k^H_{GdHL} \times K_{GdHL}$ and $k_3 = k_{GdLM} \times K^*_{GdLM}$ are characteristic for the reactions which occur by the spontaneous, proton- and metal-assisted dissociation of the $Gd(EHDTA)^-$, respectively. The rate constants, protonation and stability constants have been calculated by fitting the k_d values in Figures S19 and S20 to the Eq. (S17) and the values obtained are compared with the corresponding values of $Gd(OBETA)^-$, Gd(DTPA-BMA) and $Gd(DTPA)^{2-}$ in Table 1. The k_0 values obtained in the fitting procedures are very low and the error in them is very high, indicating the unimportance of the spontaneous dissociation of the $Gd(EHDTA)^-$.

Transchelation of the Gd(EHDTA)$^-$ with TTHA in the presence of phosphate, carbonate and citrate

In order the investigate the role of endogenous ligands for the kinetic inertness of the Gd(EHDTA)$^-$ the transchelation reactions with TTHA were monitored by ^{1}H NMR relaxometry in the presence of citrate, phosphate and carbonate excess. Previous studies indicate that the transchelation rate of the Gd(III)-complexes increase with [TTHA] in the pH range 6.5 – 11.0.[12] The contribution of TTHA to the tranchelation rate of Gd(EHDTA)$^-$ should be minimized in order to obtain reliable kinetic data for the catalytic effect of citrate, phosphate and carbonate ions. By taking into account the protonation constant of EHDTA and TTHA (Table S1), stability and protonation constants of Gd(EHDTA)$^-$ (Table S2) and Gd(TTHA)$^{3-}$ complexes (Gd(TTHA): logK_{GdL}=23.53 (1), log$K_{Gd(HL)}$=4.55 (1), log$K_{Gd(H2L)}$=2.52 (1), logK_{Gd2L}=3.63 (2) and log$K_{Gd2(HL)}$=3.57 (2), 0.1 M KCl, 25°C) model calculations were performed in Gd^{3+} - EHDTA^{4-} - TTHA^{6-} systems (Figure S21).

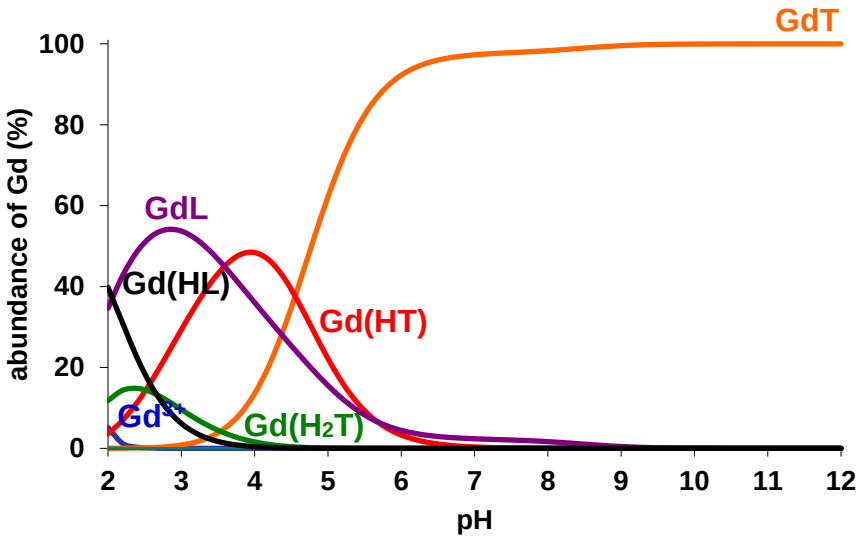

Figure S21. Species distribution of Gd^{3+} - EHDTA^{4-} ("L") - TTHA^{6-} ("T") system as a function of pH ([GdL]=1.0 mM, [TTHA]=2.0 mM, 0.1 M KCl, 25°C)

Based on our model calculations, the transchelation between Gd(EHDTA)$^-$ and TTHA takes place with 100% conversion even in the presence of 2 fold TTHA excess (Figure S21) due to the large difference between the stability constant of Gd(EHDTA)$^-$ and Gd(TTHA)$^{3-}$. Therefore, the kinetic inertness of the Gd(EHDTA)$^-$ had been studied by following the transchelation reactions with TTHA in the pH range 6.0 – 10.0 in the presence of 2 fold TTHA, 0 – 8 fold citrate, 0 – 9 fold phosphate and 0 – 30 fold carbonate excess ([GdL]$_t$ =

1.0 mM, $[TTHA]_t$=2.0 mM, $[Cit^{3-}]_t$=0 – 8 mM, $[PO_4^{3-}]_t$=0 – 9 mM, $[CO_3^{2-}]_t$=0 – 30 mM, 0.1 M KCl, 25°C).

$Gd(EHDTA)^- + TTHA^{6-} + X \rightleftharpoons Gd(TTHA)^{3-} + EHDTA^{4-} + X$ *(S18)*

where X=Cit^{3-}, PO_4^{3-} and CO_3^{2-} -ions. Relaxivity values of the $Gd(EHDTA)^-$ - $TTHA^{6-}$ reacting system in the presence of citrate is shown in Figure S22.

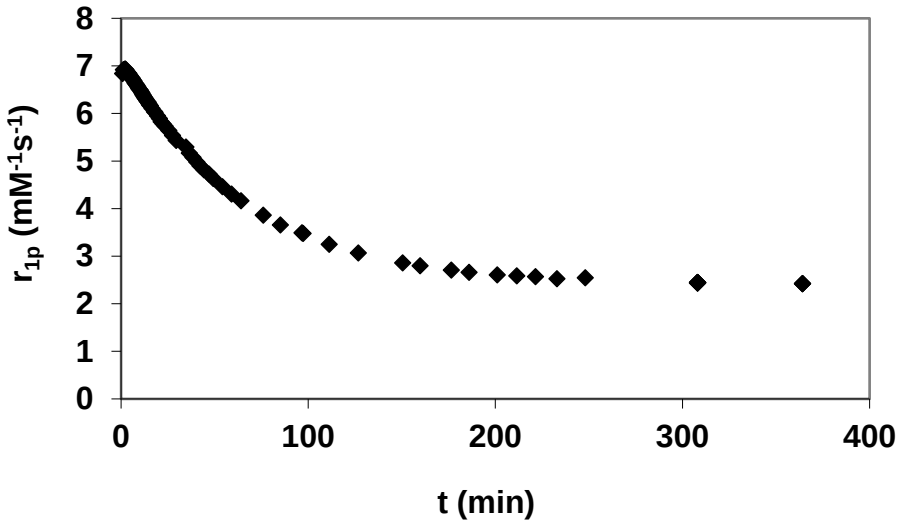

Figure S22. Relaxivity values of the Gd(EHDTA) - $TTHA^{6-}$ reacting system in the presence of citrate ($[Gd(EHDTA)^-]$=1.0 mM, $[TTHA^{6-}]$=2.0 mM, $[Cit^{3-}]_t$=2.0 mM, 0,1 M KCl, 20 MHz, pH=6.5)

In Figure S22 the relaxivity (r_{1p}) values of Gd(EHDTA) - $TTHA^{6-}$ reacting system decrease as a function of time due to the dissociation of $Gd(EHDTA)^-$ and the formation of Gd(TTHA) ($Gd(EHDTA)^-$: r_{1p}=7.2 $mM^{-1}s^{-1}$, $Gd(TTHA)^{3-}$: r_{1p}=2.4 $mM^{-1}s^{-1}$, 20 MHz, 25 °C, 0.1 M KCl). The kinetic studies of the tranchelation reactions between Gd(DTPA) derivatives and TTHA reveal that the exchange reactions takes place by the formation of ternary $[Gd(L)H_xTTHA]$ x=1 – 3 ternary species. The stability of ternary $[Gd(L)H_xTTHA]$ intermediate is very low, and the dissociation of TTHA from the latter is very probable. However, it might be assumed that the intramolecular rearrangement of ternary $[Gd(L)H_xTTHA]$ intermediate is presumably fast and the donor atoms in the GdL complex can be slowly substituted by the second and then further donor atom of TTHA step by step, whereas the whole coordinated L ligand is displaced by the TTHA, which leads to the formation of the $Gd(TTHA)^{3-}$ complex.[12] The pseudo-first-order rate constants (k_d)

characterizes the transchelation reactions between Gd(EHDTA)$^{-}$ and TTHA^{6-} as a function of pH are shown in Figure S23.

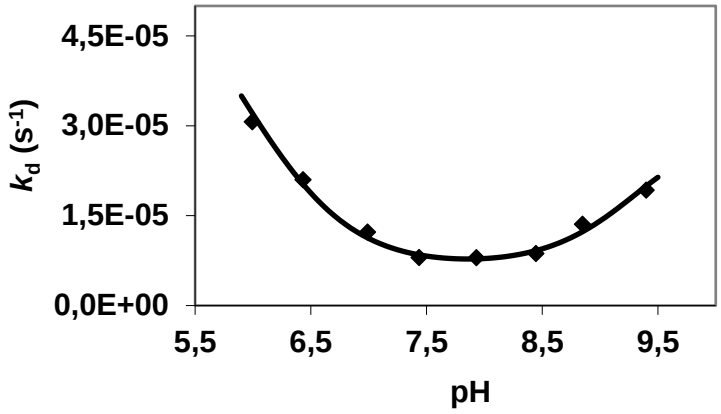

Figure S23. Pseudo-first-order rate constants (k_d) characterizes the transchelation reactions between Gd(EHDTA)$^{-}$ and TTHA^{6-} as a function of pH. ([Gd(EHDTA)]=1.0 mM, [TTHA]=2.0 mM, 0.1 M KCl, 25 °C)

The k_d values obtained for the reactions of Gd(EHDTA)$^{-}$ with TTHA in pH range 6.0 – 9.5 vary according to minimum curves, with minima at a pH of about 8.0. Based on the protonation constants of TTHA (Table S1), the mono-, di- and triprotonated TTHA ligands predominate in the pH range 6.0 – 9.5. Similarly to that of Gd(DTPA) derivatives, the ligand exchange reactions between Gd(EHDTA)$^{-}$ and $H_xTTHA^{(6-x)-}$ takes place by the formation of $\{[Gd(EHDTA)]H_xTTHA\}^{[-(6-x)-1]}$ intermediate with mono-, di- and triprotonated TTHA ligand in which the donor atoms of the TTHA ligand slowly displace the coordinated donor atoms of the EHDTA ligand in the pH range 6.0 – 9.5 (Eq. (S19)).

$$Gd(EHDTA)^{-} + H_xTTHA^{-(6-x)} \underset{K_{H3L}}{\overset{K_{HL},\, K_{H2L}}{\rightleftharpoons}} \{[Gd(EHDTA)]\, H_xTTHA\}^{[-(6-x)-1]} \xrightarrow[k_{H3L}]{k_{HL},\, k_{H2L}} Gd(TTHA)^{3-} + H_xEHDTA^{-(4-x)} \qquad (S19)$$

$$K_{H_xL} = \frac{[Gd(EHDTA)H_xTTHA]}{[Gd(EHDTA)][H_xTTHA]} \qquad x=1,\ 2 \text{ and } 3$$

where K_{HL}, K_{H2L}, K_{H3L}, k_{HL}, k_{H2L} and k_{H3L} are the equilibrium and rate constants characterizes the formation and the rearrangement of $\{[Gd(EHDTA)]\, H_xTTHA\}^{[-(6-x)-1]}$ intermediate with mono-, di- and triprotonated TTHA ligand to the final Gd(TTHA)$^{3-}$ complex. By taking into account all the possible pathways, the rate of the transchelation between Gd(EHDTA)$^{-}$ and TTHA can be expressed by Eq. (S20).

$$-\frac{d[\mathrm{GdL}]}{dt} = k_d[\mathrm{GdL}]_t = k_{\mathrm{HL}}[\mathrm{GdL(HTTHA)}] + k_{H_2L}[\mathrm{GdL(H_2TTHA)}] + k_{H_3L}[\mathrm{GdL(H_3TTHA)}] \quad (S20)$$

where [GdL(HxTTHA)] is the concentration of the intermediate formed with the mono-, di- and triprotonated TTHA ligand. By taking into account the total concentration of the Gd(III)-complex ($[GdL]_t$= [GdL] + $[GdL(HTTHA)]^{6-}$ + $[GdL(H_2TTHA)]^{5-}$ + $[GdL(H_3TTHA]^{4-}$)), the equations defining the protonation constant of the TTHA ligand (Eq. (S1), the protonation constants of TTHA ligand (Table S1), the equations defining the stability constant of the ternary {[Gd(EHDTA)] $H_xTTHA\}^{[-(6-x)-1]}$ intermediates (Eq. (S19)) and Eq. (S20), the pseudo-first-order rate constant can be expressed as follows:

$$k_d = \frac{k_1[\mathrm{HTTHA}]+k_2[\mathrm{H_2TTHA}]+k_3[\mathrm{H_3TTHA}]}{1+K_{\mathrm{HL}}[\mathrm{HTTHA}]+K_{H_2L}[\mathrm{H_2TTHA}]+K_{H_3L}[\mathrm{H_3TTHA}]} \quad (S21)$$

where $k_1 = k_{HL} \times K_{HL}$, $k_2 = k_{H2L} \times K_{H3L}$ and $k_3 = k_{H3L} \times K_{H3L}$ are characteristic for the transformation of {[Gd(EHDTA)] $H_xTTHA\}^{[-(6-x)-1]}$ intermediates with mono-, di- and triprotonated inrtmediates to the final $Gd(TTHA)^{3-}$ complex, respectively. Since the stability of the {[Gd(EHDTA)]$H_xTTHA\}^{[-(6-x)-1]}$ intermediates is very low (1>>K_{HL}[HTDITA]+ K_{HL}[H_2TDITA]+K_{H3L}[H_3TDITA], the denominator of Eq. (S21) can be neglected:

$$k_d = k_1[\mathrm{HTTHA}] + k_2[H_2\mathrm{TTHA}] + k_3[H_3\mathrm{TTHA}] \quad (S22)$$

The k_1, k_2 and k_3 rate constants characterizing the transchelation reactions of $Gd(EHDTA)^-$ with mono-, di and triporotonated TTHA have been calculated by fitting the k_d values in Figure S23 to the Eq. (S22) and the values obtained are compared with the corresponding values of $Gd(DTPA)^{2-}$, $Gd(BOPTA)^{2-}$ and Gd(DTPA-BMA) complexes in Table S4.

Comparison of k_1, k_2 and k_3 rate constants presented in Table S4 reveal that the mono-, di- and triprotonated TTHA assisted transmetallation of $Gd(EHDTA)^-$ is about 32 and 54, 6 and 10, 10 and 13 times faster than that of $Gd(DTPA)^{2-}$ and $Gd(BOPTA)^{2-}$ complexes. Since the Gd(III) ion is seven and eight coordinated in Gd(EHDTA), $Gd(DTPA)^{2-}$ and $Gd(BOPTA)^{2-}$ complexes, it can be assumed that the displacement of the EHDTA ligand with TTHA is more probable (more rapid) in [Gd(EHDTA)]$H_xTTHA\}^{[-(6-x)-1]}$ intermediates than in those intermediates of $Gd(DTPA)^{2-}$ and $Gd(BOPTA)^{2-}$ due to the weaker interactions of Gd(III) ion with EHDTA than with DTPA and BOPTA ligands. Interestingly, the mono- and diprotonated TTHA assisted transmetallation of Gd(DTPA-BMA) is significantly faster than those of $Gd(EDHTA)^-$, which might be explained by the stronger interaction of Gd(III) ion with EHDTA ligand than with the DTPA-BMA due to the presence of the two weakly coordinated amide-O donor atoms.

Table S4. Rate constants characterizing the transchelation reactions of $Gd(EHDTA)^-$-, $Gd(DTPA)^{2-}$, $Gd(BOPTA)^{2-}$ and Gd(DTPA-BMA) complexes with mono-, di- and triprotonated TTHA ligand (25 °C)

	$Gd(EHDTA)^-$	**$Gd(DTPA)^{2-}$ [a]**	**$Gd(BOPTA)^{2-}$ [a]**	**Gd(DTPA-BMA) [a]**
I	**0.1 M KCl**		**0.15 M NaCl**	
k_1 **($M^{-1}s^{-1}$)**	$(1.9 \pm 0.1)\times10^{-2}$	5.9×10^{-4}	3.5×10^{-4}	0.58
k_2 **($M^{-1}s^{-1}$)**	$(3.1 \pm 0.2)\times10^{-3}$	5.6×10^{-4}	3.1×10^{-4}	1.1×10^{-2}
k_3 **($M^{-1}s^{-1}$)**	$(2.3\pm 0.2)\times10^{-2}$	2.2×10^{-3}	1.8×10^{-3}	–

[a] Ref. [12]

The transmetallation reactions of $Gd(EHDTA)^-$ with TTHA in the presence of citrate, phosphate and carbonate ions have been investigated by ^1H NMR relaxometry in the pH range 6.0 – 10.0. The pseudo-first-order rate constants characterize the transmetallation reactions in the $Gd(EHDTA)^-$ - TTHA – Cit, $Gd(EHDTA)^-$ - TTHA – PO_4 and $Gd(EHDTA)^-$ - TTHA – CO_3 reacting systems are shown in Figures S24 – S26.

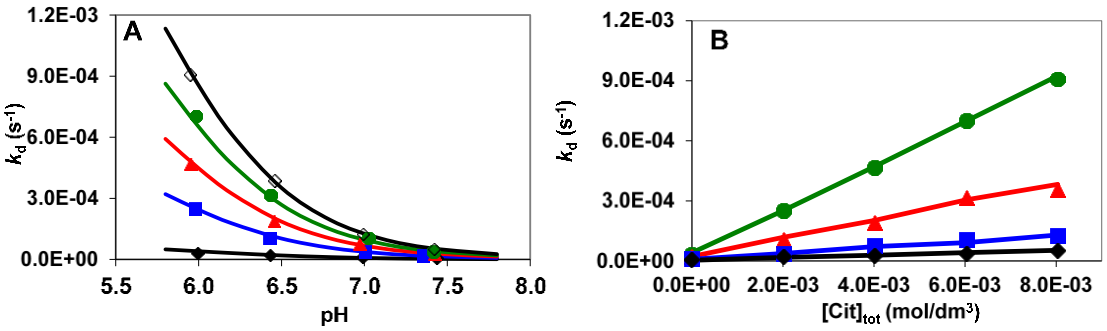

Figure S24. The pseudo-first-order rate constants characterize the transmetallation reactions in the $Gd(EHDTA)^-$ - TTHA – Cit system as a function of pH and [Cit] ($[Gd(EHDTA)^-]$=1.0 mM, $[TTHA^{6-}]$=2.0 mM, A: $[Cit]_t$=0.0 mM (♦), 2.0 mM (■), 4.0 mM (▲), 6.0 mM (●) and 8.0 mM (◊); B: pH=6.0 (●), 6.5 (▲), 7.0 (■) and 7.5 (♦), 0.1 M KCl, 25 °C)

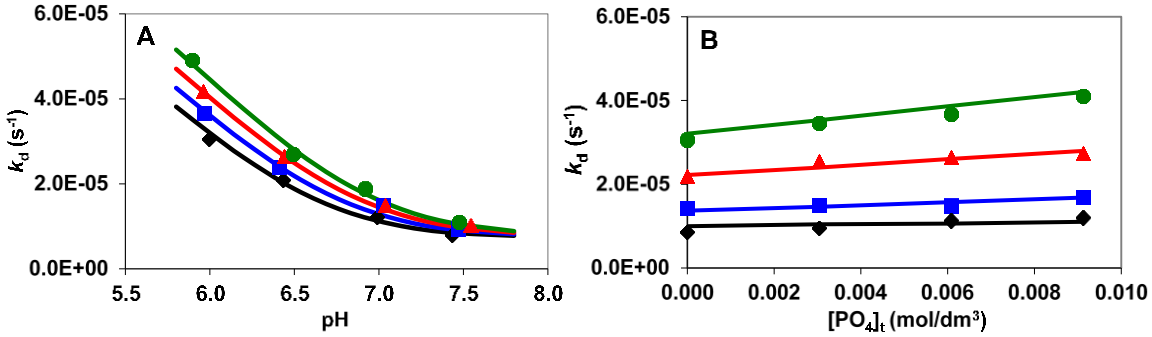

Figure S25. The pseudo-first-order rate constants characterize the transmetallation reactions in the Gd(EHDTA)$^-$ - TTHA – PO_4 system as a function of pH and $[PO_4]_t$ ([Gd(EHDTA)$^-$]=1.0 mM, [TTHA^{6-}]=2.0 mM, A: $[PO_4]_{tot}$=0.0 (♦), 3.0 (■),6.0 (▲) and 9.0 mM (●); B: pH=6.0 (●), 6.5 (▲), 7.0 (■) and 7.5 (♦), 0.1 M KCl, 25 °C)

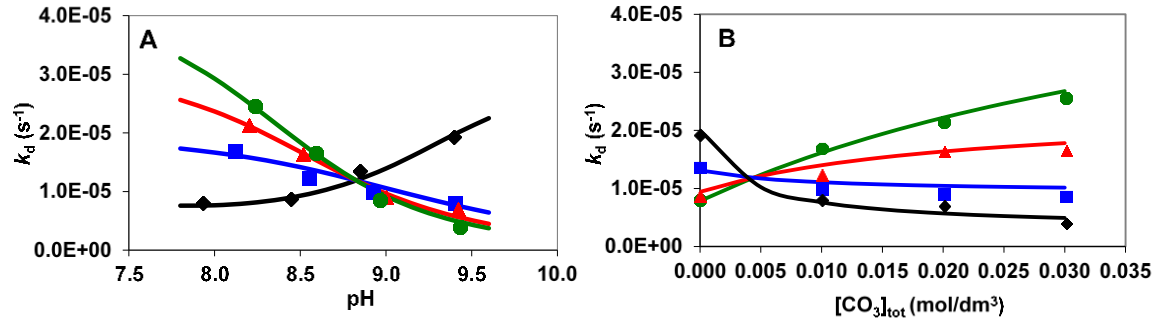

Figure S26. The pseudo-first-order rate constants characterize the transmetallation reactions in the Gd(EHDTA)$^-$ - TTHA – CO_3 system as a function of pH and $[CO_3]_t$ ([Gd(EHDTA)$^-$]=1.0 mM, [TTHA^{6-}]=2.0 mM, A: $[CO_3]_{tot}$=0.0 (♦), 10.0 (■), 20.0 (▲) and 30.0 mM (●); B: pH=8.0 (●), 8.5 (▲), 9.0 (■) and 9.5 (♦), 0.1 M KCl, 25 °C).

k_d rate constants in Figure S24 reveals that the rate of the tranchelation between Gd(HEDTA)$^-$ and TTHA in the presence of citrate increases with $[Cit]_t$ and with the lowering of pH in the pH range 6.0 – 7.5. By taking into account the protonation constants of citrate obtained by pH potentiometry (Table S5), it can be assumed that transchelation reactions of Gd(EHDTA)$^-$ is assisted by deprotonated Cit^{3-} (k_{Cit}) and HCit^{2-} ligands (k_{HCit}) predominated in the pH range 6.0 – 7.5.

Table S5. Protonation constants of $Citrate^{3-}$, PO_4^{3-} and HCO_3^- ions (0.1 M KCl, 25 °C)

	$H_3Citrate$	H_3PO_4	HCO_3^-
$\log K_1^H$	5.70 (1)	11.58 (1)	9.87 (2)
$\log K_2^H$	4.36 (1)	6.69 (1)	–
$\log K_3^H$	2.92 (1)	1.80 (1)	–

Rates (k_d) of the tranchelation reactions between $Gd(EHDTA)^-$ and TTHA increase with the decrease of the pH and with the increase of $[PO_4]_t$ (Figure S25) in the pH range 6.0 – 7.5. Moreover, the k_d values in Figure S25 are independent from the $[PO_4]_t$ at pH>7.5. Considering the protonation constants of PO_4^{3-} (Table S5) and the k_d values as a function of pH in Figure S25A, it can be assumed that the $H_2PO_4^-$ might assisted the transchelation of $Gd(EHDTA)^-$ with TTHA (k_{H2PO4}), whereas the HPO_4^{2-} predominated at pH>7.5 has practically no role for the rate of the reactions.

The k_d rate constants of the transmetallation reaction between $Gd(EHDTA)^-$ and TTHA in the presence of CO_3^{2-} increase with $[CO_3^{2-}]_t$ at pH=8.0 (Figure S26). However, the k_d values in Figure S26A decreases with the increase of $[CO_3^{2-}]_t$ at pH=9.5. According to the protonation constant of CO_3^{2-} ion, HCO_3^- predominates at pH=8.0, whereas the formation of CO_3^{2-} takes place at pH>8.5. The increase of k_d values at pH≤9.0 can be interpreted by the HCO_3^- assisted tranchelation reaction of $Gd(EHDTA)^-$ with TTHA (k_{HCO3}). At pH>9.0, the presence of CO_3^{2-} results in the formation of the ternary $[Gd(EHDTA)CO_3]^{3-}$ complex via the substitution of one or both inner-sphere water molecule. The formation of similar ternary $[Ln(OBETA)CO_3]^{3-}$ and $[Ln(DTPA\text{-}BMA)CO_3]^{2-}$ complexes have been detected by X-rays diffraction studies in solid state and by ^1H and ^{13}C NMR spectroscopy in solution.[3,13,14] Decrease of the k_d values at pH>9.0 in Figure S26B can be interpreted by the equilibrium formation ($K_{Gd(L)CO3}$) and the slow dissociation (k_{CO3}) of the $[Gd(EHDTA)CO_3]^{3-}$, which is significantly slower than the HCO_3^- assisted transchelation (k_{HCO3}) of the $Gd(EHDTA)^-$ with TTHA ligand.

By taking into account all possible pathways, the transchelation reaction of Gd(EHDTA) with TTHA can takes place with the assistance of Cit^{3-}-, $HCit^{2-}$-, $H_2PO_4^-$-, HCO_3^-- and CO_3^{2-}-ions via the formation of ternary [Gd(EHDTA)X] species. In the ternary [Gd(EHDTA)X] species, the electrostatic repulsion between the negatively charged donor atoms results in the fast rearrangement and the rapid dissociation of the Gd(III) complex to the free EHDTA ligand and Gd^{3+} ion, which react rapidly with the exchanging TTHA ligand. Moreover, the

proton transfer in the ternary [Gd(EHDTA)X] species formed with $HCit^{2-}$-, H_2Cit^--, $H_2PO_4^-$- and HCO_3^--ions is also probable via the formation of protonated Gd(HEHDTA) complex characterized by significantly lower kinetic inertness than that of the $Gd(EHDTA)^-$. By taking into account all proposed pathways, the rate of the transchelation reaction between $Gd(EHDTA)^-$ and TTHA in the presence of citrate, phosphate and carbonate can be expressed by Eq. (S23).

$$-\frac{d[\mathrm{GdL}]_{\mathrm{tot}}}{dt} = (k_1[H^+] + k_{\mathrm{cit}}[\mathrm{Cit}^{3-}] + k_{\mathrm{HCit}}[\mathrm{HCit}^{2-}] + k_{H_2\mathrm{Cit}}[H_2\mathrm{Cit}^-] + k_{\mathrm{CO3}}[\mathrm{CO_3}^{2-}] + \\ + k_{\mathrm{HCO_3}}[\mathrm{HCO_3}^-] + k_{H_2\mathrm{PO_4}}[H_2\mathrm{PO_4}] + k_{\mathrm{HL}}[\mathrm{HTTHA}] + k_{H_2L}[H_2\mathrm{TTHA}] + \\ + k_{H_3L}[H_3\mathrm{TTHA}])[\mathrm{GdL}] \qquad (S23)$$

In our experimental condition ($[GdL]_t$ = 1.0 mM, $[TTHA]_t$=2.0 mM, $[Cit^{3-}]_t$=0 – 8 mM, $[PO_4^{3-}]_t$=0 – 9 mM, $[CO_3^{2-}]_t$=0 – 30 mM, pH=6.0 – 10.0, 0.1 M KCl, 25°C), the formation of ternary [Gd(EHDTA)X] species takes place with CO_3^{2-} ion in considerable amount. By taking into account the total concentration of the $Gd(EHDTA)^-$ complex ($[GdL]_t=[GdL]+[Gd(L)CO_3]$), stability constant of the ternary $[Gd(EHDTA)CO_3]^{3-}$ species ($K_{Gd(L)CO3}=[Gd(L)CO_3)^{3-}]/[GdL^-][CO_3^{2-}]$) and Eq. (S23), the pseudo-first-order rate constant can be expressed as follows:

$$k_d = \frac{k_{Cit}[Cit^{3-}]+k_{HCit}[HCit^{2-}]+k_{CO_3}[CO_3{}^{2-}]+ \\ +k_{HCO_3}[HCO_3{}^-]+k_{H_2PO_4}[H_2PO_4{}^-]+k_{HL}[HTTHA]+k_{H_2L}[H_2TTHA]+k_{H_3L}[H_3TTHA]}{1+K_{GdL(CO_3)}[CO_3{}^{2-}]} \qquad (S24)$$

The rate constants characterizing the rate of the Cit^{3-}-, $HCit^{2-}$-, H_2Cit^--, $H_2PO_4^-$-, HCO_3^-- and CO_3^2-ion assisted transchelation reactions between $Gd(EHDTA)^-$ and TTHA have been calculated by fitting the k_d values in Figures S24-S26 to Eq. (S24) by taking into account the rate of the pure TTHA mediated transchelation of $Gd(EHDTA)^-$ (Table S4) and the speciation of the citrate, phosphate and carbonate in the pH range 6.0 – 10.0 (Table S5). The rate and equilibrium constants of the Cit^{3-}-, $HCit^{2-}$-, H_2Cit^--, $H_2PO_4^-$-, HCO_3^-- and CO_3^2-ion assisted transchelation reactions of $Gd(EHDTA)^-$ are compared with the corresponding values of $Gd(OBETA)^-$, Gd(DTPA-BMA) and $Gd(DTPA)^{2-}$ in Table 1. The k_{Cit} and k_{CO3} values obtained in the fitting procedures are very low and the error in them is very high, indicating the negligible contribution of the Cit^{3-} and CO_3^{2-} ions to the dissociation of the $Gd(EHDTA)^-$ in our experimental condition.

^{1}H NMR relaxometric data

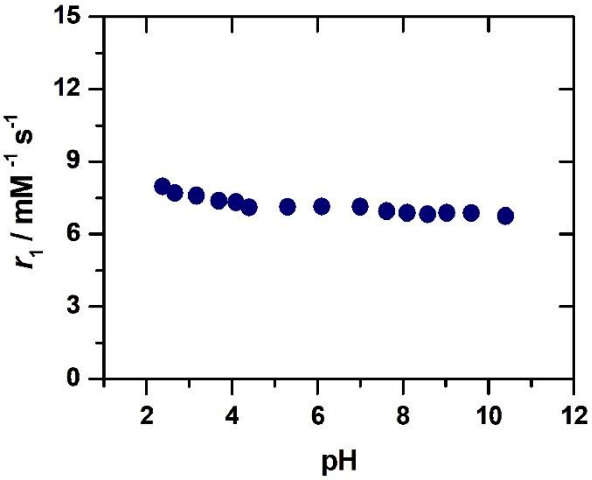

Figure S27. pH dependency of r_1 of Gd(EHDTA)$^-$ at 32 MHz and 298 K in aqueous solution**.**

Photoluminescence measurements

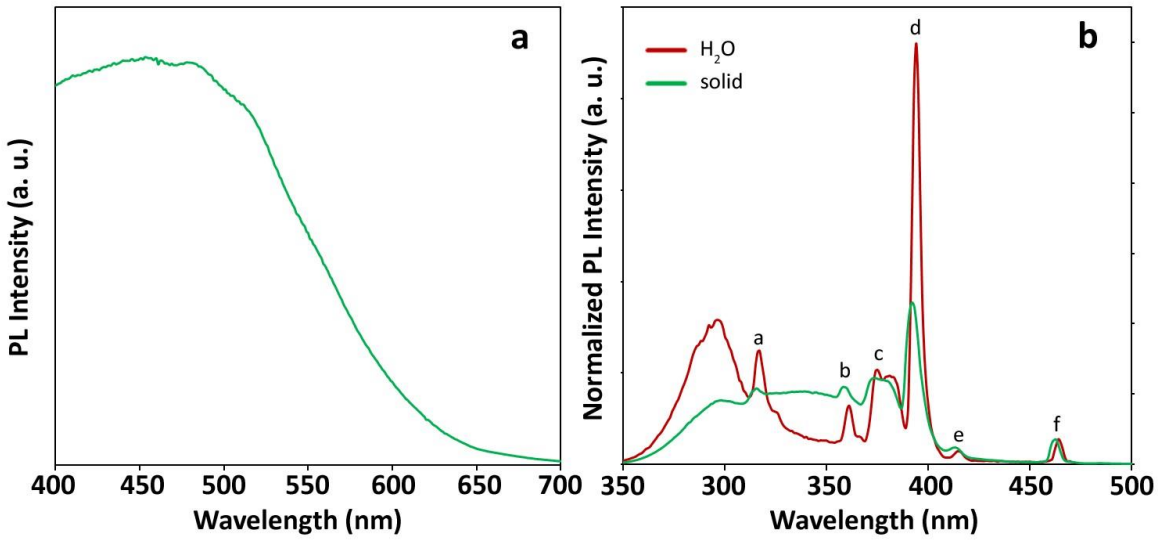

Figure S28. a. PL spectrum of a water solution of Gd(EHDTA)$^-$ excited at 280 nm and showing a broad band attributable to ligand-centered emission. b. Normalized excitation (PLE) spectra of Eu(EHDTA)$^-$ in the solid state (green) and in water solution (red), monitored at 617 and 615 nm, respectively. Labels indicate the Eu^{3+}-centred excitation peaks as assigned in Table S6.

Table S6: Assignment of labelled PLE peaks for Eu(EHDTA)$^-$.[15]

Label	Wavelength (nm)[#]	Wavenumber (cm^{-1})[#]	Transition
		Excitation	
a	316	31646	$^5H_6 \leftarrow {}^7F_0$
b	359	27855	$^5D_4 \leftarrow {}^7F_0$
c	372	26882	$^5L_7, ^5G_5 \leftarrow {}^7F_1$ / $^5G_{2,4,6} \leftarrow {}^7F_0$
d	393	25445	$^5L_6 \leftarrow {}^7F_0$
e	414	24155	$^5D_3 \leftarrow {}^7F_1$
f	462	21645	$^5D_2 \leftarrow {}^7F_0$

[#]Referred to the spectrum of the sample in water solution.

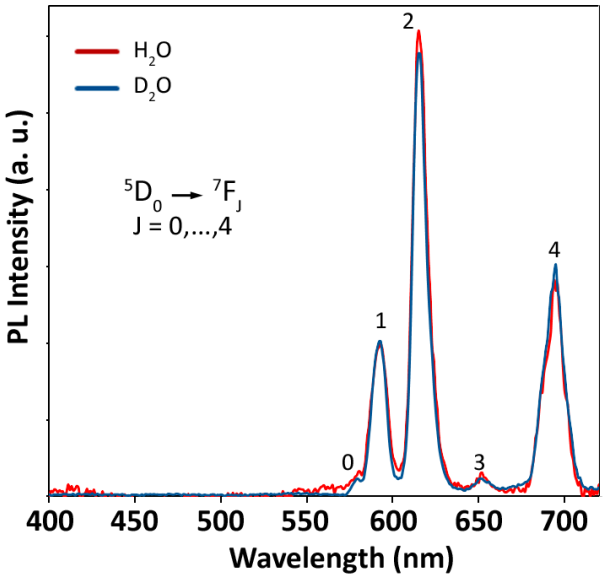

Figure S29. PL spectra of Eu(EHDTA)$^-$ in H_2O (red) and D_2O (blue) solution after spectral deconvolution and subtraction of the ligand contribution. Spectra are herein normalized to the $^5D_0 \rightarrow {}^7F_1$ emission line at 593 nm.

Radiative rate constant

The radiative rate constant k_{RAD}, was calculated from the Einstein's equation for spontaneous emission:[16]

$$\frac{1}{\tau_{RAD}} = k_{RAD} = A_{MD} n^3 \frac{I_{TOT}}{I_{MD}}$$

where the radiative lifetime, τ_{RAD} is the "natural" radiative lifetime that the emitter would display in the absence of quenching phenomena. $A_{MD,0}$ is the spontaneous emission probability for the purely magnetic dipole $^5D_0 \rightarrow {}^7F_1$ transition (which is independent of the coordination environment) of Eu^{3+} in vacuum which takes a value of 14.65 s^{-1}. I_{TOT}/I_{MD} is the ratio of the total integrated area of the Eu^{3+} PL spectrum to the area of the $^5D_0 \rightarrow {}^7F_1$ line. *n* is the refractive index of the medium whose value was taken as 1.33 for water and deuterated water and as 1.5 for the solid state sample.

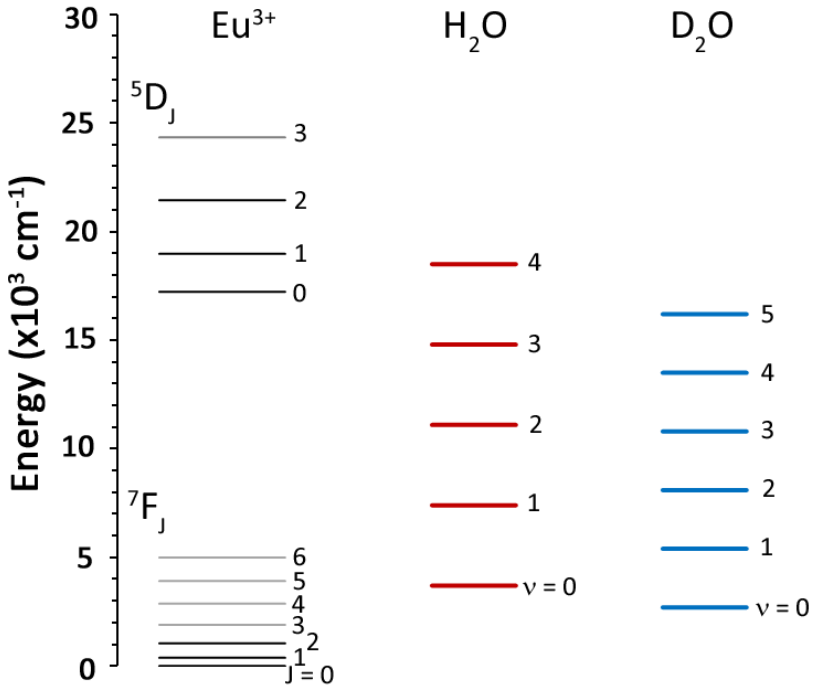

Figure S30. Diagram of the ^5D_J (J = 0,…,3) and ^7F_J (J = 0,…,6) energy level manifolds of Eu^{3+} compared to the energy of the stretching vibrational modes ($\nu_{sym}+\nu_{antisym}$) of H_2O and D_2O molecules and their superior harmonics. Vibrational energy refers to the free molecules in the condensed phase.

Time resolved data.

Time-resolved data were fitted with mono-exponential (i = 1) or bi-exponential (i = 1, 2) equations:

$$I(t) = \sum_i A_i e^{-t/\tau_i}$$

Where τ_i is the decay time constant and A_i is a pre-exponential factor or amplitude.

For bi-exponential decays, average decay time constants or lifetimes were calculated according to two models. The first is the *intensity average lifetime*:

$$\tau_{intensity} = \frac{\sum A_i \tau_i^2}{\sum A_i \tau_i}$$

The second model is the *amplitude average lifetime*:

$$\tau_{amplitude} = \frac{\sum A_i \tau_i}{\sum A_i}$$

where the contribution (%) of each *i*-th decay component is expressed by:

$$\% = \frac{A_i}{\sum A_i} \times 100$$

The two models are conceptually different since the *intensity average lifetime* refers to a collection of emitters and expresses the average amount of time a fluorophore spends in the excited state. On the other hand, the *amplitude average lifetime* is the lifetime an emitter would have if it had the same steady state fluorescence as the emitter with multiple lifetimes.[17] $\tau_{amplitude}$ is directly proportional to quantum yields and amplitude or pre-exponential factors A_i are proportional to the fraction of emitters decaying with the time constant τ_i. For this reason, the contribution of the different population of emitters to the decay signal was herein calculated based on the *amplitude average lifetime*. Instead, the *intensity average lifetime* was deemed the most correct to retrieve the number of coordinated water molecules through Horrock's equation $q = A(\kappa_{H2O}-\kappa_{D2O})$ (with A = 1.05 ms), where $\kappa_{H2O} = 1/\tau_{intensity}(H_2O)$.

X-Ray diffractometric studies of the ternary $[Gd(EHDTA)CO_3]^{3-}$ complex

Single crystal X-ray diffraction (SC-XRD) data were collected with a Smart APEXII CCD area-detector diffractometer (BRUKER). The radiation source was a molybdenum anode (Mo-Kα, λ=0.71073 Å) with the generator working at 50 kV and 30 mA. The data reduction was carried out with CrysAlis Pro[18] version 1.171.42.60a using an empirical absorption correction with spherical harmonics (SCALE3 ABSPACK). The structure was solved by dual space methods with SHELXT-2015[19] and refined with SHELXL-2018[20] using the WinGX program suite[21]. Structure refinement was done using full-matrix least-square routines against F^2. All hydrogen atoms were detected as peaks in the residual electron

density map. Hydrogen atoms in the ligand were modelled on idealized positions. Hydrogen atoms in the guanidinium ions and water molecules were refined freely only using soft restraints. The pictures were generated with the programs ORTEP-3[21] (representation with anisotropic displacement parameters), MERCURY[22] (hydrogen bonding network). Hydrogen atoms were omitted for clarity in these representations. CCDC 2235393 ($[C(NH_2)_3]_3[Gd(EHDTA)(CO_3)]\cdot 2H_2O$) contains the supplementary crystallographic data for this paper. These data can and additional information can be obtained free of charge via https://summary.ccdc.cam.ac.uk/structure-summary-form (or from the Cambridge Crystallographic Data Centre, 12 Union Road, Cambridge CB2 1EZ, UK; fax: (+44)1223-336-033; or deposit@ccdc.cam.uk).

Table S7. Summary of crystallographic data and refinement details for $C(NH_2)_3]_3[Gd(EHDTA)(CO_3)]\cdot 2H_2O$

CCDC No.	2235393
Formula	$C_{18}H_{40}GdN_{11}O_{14}$
Formula weight	791.86
Crystal system	Monoclinic
Space group	$P2_1/n$
a [Å]	10.0882(2)
b [Å]	14.8564(2)
c [Å]	20.7254(3)
α [°]	90
β [°]	95.4430(10)
γ [°]	90
V [Å^3]	3092.20(9)
Z	4
Radiation type	Mo-Kα
Temp. [K]	298(2)
$\rho_{(calcd)}$ [g·cm^{-3}]	1.701
μ [mm^{-1}]	2.225
F(000)	1604
Cryst. size [mm^3]	0.200 x 0.050 x 0.030
θ range [°]	1.689-28.281
Limiting indices	-13<=h<=13 -19<=k<=19 -27<=l<=27
Reflections collected/unique[a]	63512 / 7674 [R(int) = 0.0636]
Data/restraints/ param	7674 / 22 / 485
Completeness to θ = 25.242° [%]	100.0
Max. and min. transmission	1.00000 and 0.70031
Final R indices (I > 2σ(I))[b]	R1 = 0.0298, wR2 = 0.0648
R indices (all data)	R1 = 0.0334, wR2 = 0.0666
Goodness of fit[c] on F^2	1.075
Largest diff. peak and hole [Å^{-3}]	1.614 and -0.636

[a] $R_{int} = \Sigma|F_o^2 - F_o^2(mean)|/\Sigma F_o^2$, [b] $R_1 = \Sigma||F_o| - |F_c||/\Sigma|F_o|$, $wR_2 = \{\Sigma[w(F_o^2 - F_c^2)^2]/\Sigma[w(F_o^2)^2]\}^{1/2}$, [c] GooF = $\{S/(n-p)\}^{1/2} = \{\Sigma[w(F_o^2 - F_c^2)^2]/(n-p)\}^{1/2}$.

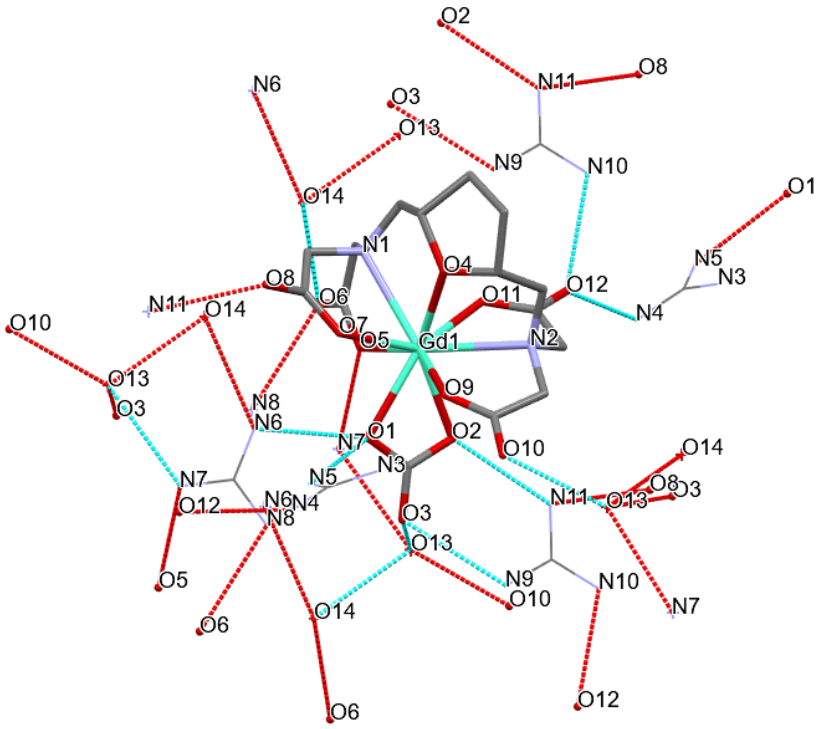

Figure S31. Hydrogen bonding network in the crystal strtuctre of $[C(NH_2)_3]_3[Gd(EHDTA)(CO_3)]\cdot 2H_2O$

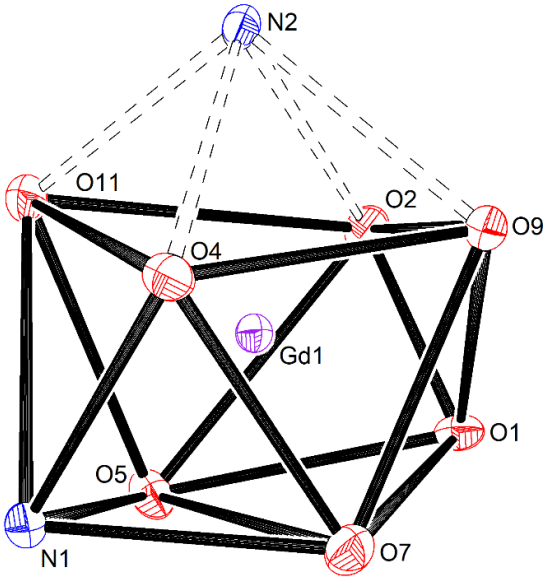

Figure S32. The coordination polyhedron around the Gd(III) ion in $[C(NH_2)_3]_3[Gd(EHDTA)(CO_3)]\cdot 2H_2O$. Distances of best planes through N1-O7-O1-O5 (Å): 0.198 (N1); 0.187 (O7); 0.178 (O1); 0.189 (O5); 0.188 (mean). Distances of best planes through O2-O11-O4-O9 [Å]: 0.157 (O2); 0.145 (O11); 0.168 (O4); 0.180 (O9); 0.163 (mean).

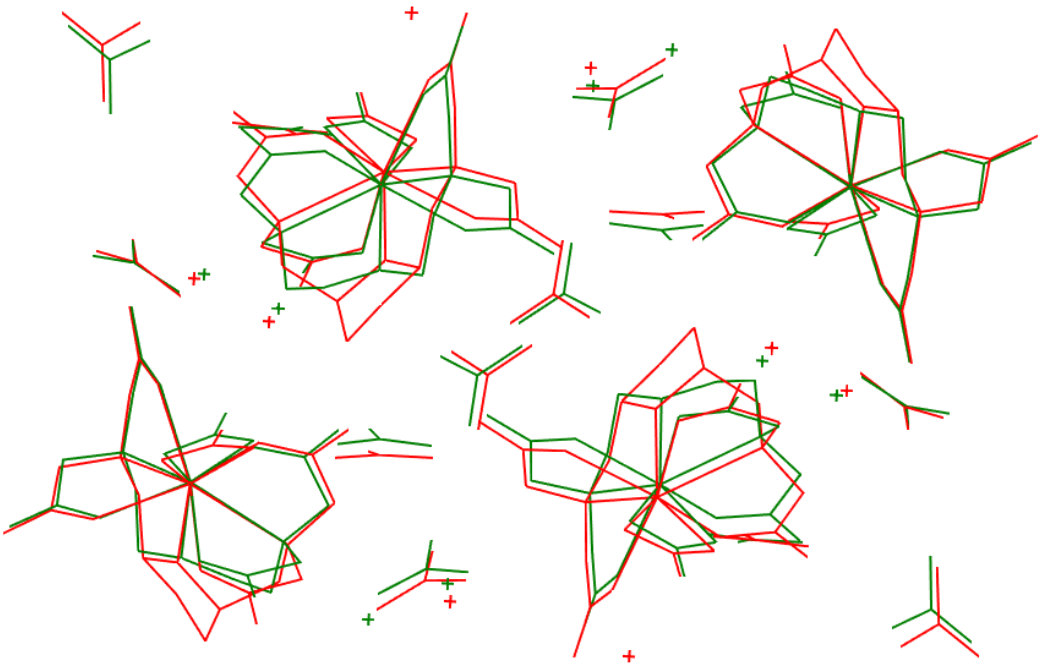

Figure S33. Overlay of crystal structures of $[C(NH_2)_3]_3[Gd(EHDTA)(CO_3)]\cdot 2H_2O$ (**red**) and isostructural $[C(NH_2)_3]_3[Lu(OBETA)(CO_3)]\cdot 2H_2O$ [3] (**green**).

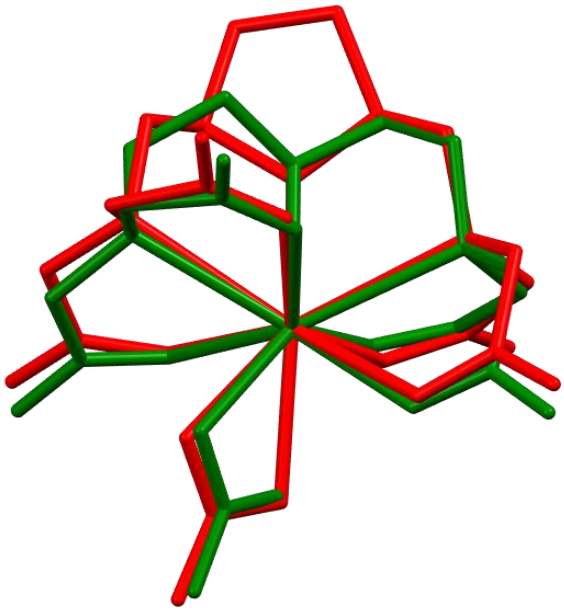

Figure S34. Overlay of molecular structures of the complex ion $[Ln(L)(CO_3)]$ of the crystal structures of $[C(NH_2)_3]_3[Gd(EHDTA)(CO_3)]\cdot 2H_2O$ (**red**) and $[C(NH_2)_3]_3[Lu(OBETA)(CO_3)]\cdot 2H_2O$[3] (**green**).

Table S8. Selected bond distances (Å) and angles (°) for $[Gd(EHDTA)(CO_3)]^{3-}$

C(9)-O(6)	1.262(3)	O(5)-Gd(1)	2.4505(18)	N(3)-C(16)-N(4)	120.1(3)	O(1)-Gd(1)-O(2)	54.34(6)
C(9)-O(5)	1.289(3)	O(7)-Gd(1)	2.4234(18)	N(3)-C(16)-N(5)	121.3(3)	O(5)-Gd(1)-O(2)	83.86(7)
C(9)-C(8)	1.547(4)	O(4)-Gd(1)	2.4793(17)	N(4)-C(16)-N(5)	118.6(3)	O(7)-Gd(1)-O(4)	72.34(6)
C(8)-N(1)	1.498(3)	O(11)-Gd(1)	2.5002(18)	N(6)-C(17)-N(7)	121.1(3)	O(9)-Gd(1)-O(4)	75.19(6)
C(11)-O(8)	1.268(3)	O(9)-Gd(1)	2.4245(17)	N(6)-C(17)-N(8)	119.5(3)	O(1)-Gd(1)-O(4)	138.72(6)
C(11)-O(7)	1.281(3)	O(2)-Gd(1)	2.4511(17)	N(7)-C(17)-N(8)	119.4(3)	O(5)-Gd(1)-O(4)	129.61(6)
C(11)-C(10)	1.536(4)	O(1)-Gd(1)	2.4429(18)	N(10)-C(18)-N(11)	120.5(3)	O(2)-Gd(1)-O(4)	143.24(6)
C(10)-N(1)	1.498(3)	O(6)-C(9)-O(5)	124.8(2)	N(10)-C(18)-N(9)	119.7(3)	O(7)-Gd(1)-O(11)	142.62(6)
C(2)-N(1)	1.515(3)	O(6)-C(9)-C(8)	118.2(2)	N(11)-C(18)-N(9)	119.8(3)	O(9)-Gd(1)-O(11)	127.84(6)
C(2)-C(3)	1.531(4)	O(5)-C(9)-C(8)	116.9(2)	C(8)-N(1)-C(10)	110.1(2)	O(1)-Gd(1)-O(11)	135.12(6)
C(3)-O(4)	1.480(3)	N(1)-C(8)-C(9)	112.1(2)	C(8)-N(1)-C(2)	110.47(19)	O(5)-Gd(1)-O(11)	78.42(7)
C(3)-C(4)	1.545(4)	O(8)-C(11)-O(7)	123.2(3)	C(10)-N(1)-C(2)	111.6(2)	O(2)-Gd(1)-O(11)	87.47(6)
C(4)-C(5)	1.552(4)	O(8)-C(11)-C(10)	118.4(2)	C(8)-N(1)-Gd(1)	108.00(15)	O(4)-Gd(1)-O(11)	85.74(7)
C(5)-C(6)	1.552(4)	O(7)-C(11)-C(10)	118.4(2)	C(10)-N(1)-Gd(1)	109.92(15)	O(7)-Gd(1)-N(1)	65.85(6)
C(6)-O(4)	1.481(3)	N(1)-C(10)-C(11)	114.2(2)	C(2)-N(1)-Gd(1)	106.62(14)	O(9)-Gd(1)-N(1)	131.62(6)
C(6)-C(7)	1.525(4)	N(1)-C(2)-C(3)	113.2(2)	C(14)-N(2)-C(12)	111.29(19)	O(1)-Gd(1)-N(1)	120.04(6)
C(7)-N(2)	1.512(3)	O(4)-C(3)-C(2)	107.98(19)	C(14)-N(2)-C(7)	108.06(19)	O(5)-Gd(1)-N(1)	64.06(6)
C(15)-O(12)	1.276(3)	O(4)-C(3)-C(4)	104.8(2)	C(12)-N(2)-C(7)	111.9(2)	O(2)-Gd(1)-N(1)	146.63(7)
C(15)-O(11)	1.282(3)	C(2)-C(3)-C(4)	113.3(2)	C(14)-N(2)-Gd(1)	107.88(15)	O(4)-Gd(1)-N(1)	65.91(6)
C(15)-C(14)	1.544(4)	C(3)-C(4)-C(5)	103.0(2)	C(12)-N(2)-Gd(1)	108.55(14)	O(11)-Gd(1)-N(1)	77.73(6)
C(14)-N(2)	1.496(3)	C(6)-C(5)-C(4)	103.9(2)	C(7)-N(2)-Gd(1)	109.03(14)	O(7)-Gd(1)-N(2)	128.33(7)
C(13)-O(10)	1.255(3)	O(4)-C(6)-C(7)	107.1(2)	C(9)-O(5)-Gd(1)	126.12(16)	O(9)-Gd(1)-N(2)	64.78(6)
C(13)-O(9)	1.291(3)	O(4)-C(6)-C(5)	104.7(2)	C(11)-O(7)-Gd(1)	127.11(17)	O(1)-Gd(1)-N(2)	120.79(6)
C(13)-C(12)	1.542(3)	C(7)-C(6)-C(5)	114.3(2)	C(3)-O(4)-C(6)	111.44(18)	O(5)-Gd(1)-N(2)	137.95(6)
C(12)-N(2)	1.499(3)	N(2)-C(7)-C(6)	112.4(2)	C(3)-O(4)-Gd(1)	124.47(14)	O(2)-Gd(1)-N(2)	78.44(6)
C(1)-O(3)	1.284(3)	O(12)-C(15)-O(11)	125.0(2)	C(6)-O(4)-Gd(1)	120.55(14)	O(4)-Gd(1)-N(2)	66.30(6)
C(1)-O(2)	1.316(3)	O(12)-C(15)-C(14)	117.1(2)	C(15)-O(11)-Gd(1)	124.48(16)	O(11)-Gd(1)-N(2)	63.09(6)
C(1)-O(1)	1.317(3)	O(11)-C(15)-C(14)	117.9(2)	C(13)-O(9)-Gd(1)	124.05(16)	N(1)-Gd(1)-N(2)	118.98(6)
C(1)-Gd(1)	2.873(2)	N(2)-C(14)-C(15)	110.6(2)	C(1)-O(2)-Gd(1)	94.55(14)	O(7)-Gd(1)-C(1)	101.17(7)
C(16)-N(3)	1.320(4)	O(10)-C(13)-O(9)	124.1(2)	C(1)-O(1)-Gd(1)	94.92(14)	O(9)-Gd(1)-C(1)	75.12(7)
C(16)-N(4)	1.344(4)	O(10)-C(13)-C(12)	117.5(2)	O(7)-Gd(1)-O(9)	75.97(6)	O(1)-Gd(1)-C(1)	27.17(6)
C(16)-N(5)	1.358(4)	O(9)-C(13)-C(12)	118.4(2)	O(7)-Gd(1)-O(1)	74.46(6)	O(5)-Gd(1)-C(1)	78.71(7)
C(17)-N(6)	1.342(4)	N(2)-C(12)-C(13)	113.9(2)	O(9)-Gd(1)-O(1)	73.52(6)	O(2)-Gd(1)-C(1)	27.18(6)
C(17)-N(7)	1.345(4)	O(3)-C(1)-O(2)	123.0(2)	O(7)-Gd(1)-O(5)	92.45(7)	O(4)-Gd(1)-C(1)	150.30(7)
C(17)-N(8)	1.355(4)	O(3)-C(1)-O(1)	120.9(2)	O(9)-Gd(1)-O(5)	148.52(6)	O(11)-Gd(1)-C(1)	112.14(7)
C(18)-N(10)	1.342(4)	O(2)-C(1)-O(1)	116.2(2)	O(1)-Gd(1)-O(5)	75.20(6)	N(1)-Gd(1)-C(1)	139.04(7)
C(18)-N(11)	1.343(4)	O(3)-C(1)-Gd(1)	177.95(19)	O(7)-Gd(1)-O(2)	127.95(6)	N(2)-Gd(1)-C(1)	99.80(6)
C(18)-N(9)	1.344(4)	O(2)-C(1)-Gd(1)	58.27(12)	O(9)-Gd(1)-O(2)	80.84(7)	O(1)-Gd(1)-O(2)	54.34(6)
N(1)-Gd(1)	2.724(2)	O(1)-C(1)-Gd(1)	57.91(12)	O(1)-Gd(1)-O(2)	54.34(6)	O(5)-Gd(1)-O(2)	83.86(7)
C(9)-O(6)	1.262(3)	O(5)-Gd(1)	2.4505(18)	O(5)-Gd(1)-O(2)	83.86(7)	O(7)-Gd(1)-O(4)	72.34(6)
C(9)-O(5)	1.289(3)	O(7)-Gd(1)	2.4234(18)	O(7)-Gd(1)-O(4)	72.34(6)	O(9)-Gd(1)-O(4)	75.19(6)
C(9)-C(8)	1.547(4)	O(4)-Gd(1)	2.4793(17)	N(3)-C(16)-N(4)	120.1(3)	O(1)-Gd(1)-O(4)	138.72(6)
C(8)-N(1)	1.498(3)	O(11)-Gd(1)	2.5002(18)	N(3)-C(16)-N(5)	121.3(3)	O(5)-Gd(1)-O(4)	129.61(6)
C(11)-O(8)	1.268(3)	O(9)-Gd(1)	2.4245(17)	N(4)-C(16)-N(5)	118.6(3)	O(2)-Gd(1)-O(4)	143.24(6)
C(11)-O(7)	1.281(3)	O(2)-Gd(1)	2.4511(17)	N(6)-C(17)-N(7)	121.1(3)	O(7)-Gd(1)-O(11)	142.62(6)
C(11)-C(10)	1.536(4)	O(1)-Gd(1)	2.4429(18)	N(6)-C(17)-N(8)	119.5(3)	O(9)-Gd(1)-O(11)	127.84(6)
C(10)-N(1)	1.498(3)	O(6)-C(9)-O(5)	124.8(2)	N(7)-C(17)-N(8)	119.4(3)	O(1)-Gd(1)-O(11)	135.12(6)
C(2)-N(1)	1.515(3)	O(6)-C(9)-C(8)	118.2(2)	N(10)-C(18)-N(11)	120.5(3)	O(5)-Gd(1)-O(11)	78.42(7)
C(2)-C(3)	1.531(4)	O(5)-C(9)-C(8)	116.9(2)	N(10)-C(18)-N(9)	119.7(3)	O(2)-Gd(1)-O(11)	87.47(6)

C(3)-O(4)	1.480(3)	N(1)-C(8)-C(9)	112.1(2)	N(11)-C(18)-N(9)	119.8(3)	O(4)-Gd(1)-O(11)	85.74(7)
C(3)-C(4)	1.545(4)	O(8)-C(11)-O(7)	123.2(3)	C(8)-N(1)-C(10)	110.1(2)	O(7)-Gd(1)-N(1)	65.85(6)
C(4)-C(5)	1.552(4)	O(8)-C(11)-C(10)	118.4(2)	C(8)-N(1)-C(2)	110.47(19)	O(9)-Gd(1)-N(1)	131.62(6)
C(5)-C(6)	1.552(4)	O(7)-C(11)-C(10)	118.4(2)	C(10)-N(1)-C(2)	111.6(2)	O(1)-Gd(1)-N(1)	120.04(6)
C(6)-O(4)	1.481(3)	N(1)-C(10)-C(11)	114.2(2)	C(8)-N(1)-Gd(1)	108.00(15)	O(5)-Gd(1)-N(1)	64.06(6)
C(6)-C(7)	1.525(4)	N(1)-C(2)-C(3)	113.2(2)	C(10)-N(1)-Gd(1)	109.92(15)	O(2)-Gd(1)-N(1)	146.63(7)
C(7)-N(2)	1.512(3)	O(4)-C(3)-C(2)	107.98(19)	C(2)-N(1)-Gd(1)	106.62(14)	O(4)-Gd(1)-N(1)	65.91(6)
C(15)-O(12)	1.276(3)	O(4)-C(3)-C(4)	104.8(2)	C(14)-N(2)-C(12)	111.29(19)	O(11)-Gd(1)-N(1)	77.73(6)
C(15)-O(11)	1.282(3)	C(2)-C(3)-C(4)	113.3(2)	C(14)-N(2)-C(7)	108.06(19)	O(7)-Gd(1)-N(2)	128.33(7)
C(15)-C(14)	1.544(4)	C(3)-C(4)-C(5)	103.0(2)	C(12)-N(2)-C(7)	111.9(2)	O(9)-Gd(1)-N(2)	64.78(6)
C(14)-N(2)	1.496(3)	C(6)-C(5)-C(4)	103.9(2)	C(14)-N(2)-Gd(1)	107.88(15)	O(1)-Gd(1)-N(2)	120.79(6)
C(13)-O(10)	1.255(3)	O(4)-C(6)-C(7)	107.1(2)	C(12)-N(2)-Gd(1)	108.55(14)	O(5)-Gd(1)-N(2)	137.95(6)
C(13)-O(9)	1.291(3)	O(4)-C(6)-C(5)	104.7(2)	C(7)-N(2)-Gd(1)	109.03(14)	O(2)-Gd(1)-N(2)	78.44(6)
C(13)-C(12)	1.542(3)	C(7)-C(6)-C(5)	114.3(2)	C(9)-O(5)-Gd(1)	126.12(16)	O(4)-Gd(1)-N(2)	66.30(6)
C(12)-N(2)	1.499(3)	N(2)-C(7)-C(6)	112.4(2)	C(11)-O(7)-Gd(1)	127.11(17)	O(11)-Gd(1)-N(2)	63.09(6)
C(1)-O(3)	1.284(3)	O(12)-C(15)-O(11)	125.0(2)	C(3)-O(4)-C(6)	111.44(18)	N(1)-Gd(1)-N(2)	118.98(6)
C(1)-O(2)	1.316(3)	O(12)-C(15)-C(14)	117.1(2)	C(3)-O(4)-Gd(1)	124.47(14)	O(7)-Gd(1)-C(1)	101.17(7)
C(1)-O(1)	1.317(3)	O(11)-C(15)-C(14)	117.9(2)	C(6)-O(4)-Gd(1)	120.55(14)	O(9)-Gd(1)-C(1)	75.12(7)
C(1)-Gd(1)	2.873(2)	N(2)-C(14)-C(15)	110.6(2)	C(15)-O(11)-Gd(1)	124.48(16)	O(1)-Gd(1)-C(1)	27.17(6)
C(16)-N(3)	1.320(4)	O(10)-C(13)-O(9)	124.1(2)	C(13)-O(9)-Gd(1)	124.05(16)	O(5)-Gd(1)-C(1)	78.71(7)
C(16)-N(4)	1.344(4)	O(10)-C(13)-C(12)	117.5(2)	C(1)-O(2)-Gd(1)	94.55(14)	O(2)-Gd(1)-C(1)	27.18(6)
C(16)-N(5)	1.358(4)	O(9)-C(13)-C(12)	118.4(2)	C(1)-O(1)-Gd(1)	94.92(14)	O(4)-Gd(1)-C(1)	150.30(7)
C(17)-N(6)	1.342(4)	N(2)-C(12)-C(13)	113.9(2)	O(7)-Gd(1)-O(9)	75.97(6)	O(11)-Gd(1)-C(1)	112.14(7)
C(17)-N(7)	1.345(4)	O(3)-C(1)-O(2)	123.0(2)	O(7)-Gd(1)-O(1)	74.46(6)	N(1)-Gd(1)-C(1)	139.04(7)
C(17)-N(8)	1.355(4)	O(3)-C(1)-O(1)	120.9(2)	O(9)-Gd(1)-O(1)	73.52(6)	N(2)-Gd(1)-C(1)	99.80(6)
C(18)-N(10)	1.342(4)	O(2)-C(1)-O(1)	116.2(2)	O(7)-Gd(1)-O(5)	92.45(7)		
C(18)-N(11)	1.343(4)	O(3)-C(1)-Gd(1)	177.95(19)	O(9)-Gd(1)-O(5)	148.52(6)		
C(18)-N(9)	1.344(4)	O(2)-C(1)-Gd(1)	58.27(12)	O(1)-Gd(1)-O(5)	75.20(6)		
N(1)-Gd(1)	2.724(2)	O(1)-C(1)-Gd(1)	57.91(12)	O(7)-Gd(1)-O(2)	127.95(6)		
N(2)-Gd(1)	2.734(2)			O(9)-Gd(1)-O(2)	80.84(7)		

Table S9. Geometrical parameters of hydrogen bonds found in the crystal packing of $[C(NH_2)_3]_3[Gd(EHDTA)(CO_3)]\cdot 2H_2O$

D-H...A	d(D-H)	d(H...A)	d(D...A)	<(DHA)
N(4)-H(4C)...O(12)#1	0.863(18)	2.17(2)	3.005(3)	162(3)
N(5)-H(5C)...O(1)	0.859(19)	2.09(3)	2.870(3)	151(4)
N(6)-H(6D)...O(1)	0.865(18)	2.00(2)	2.845(3)	164(3)
N(6)-H(6C)...O(14)#2	0.865(18)	2.207(19)	3.057(4)	167(3)
N(7)-H(7D)...O(5)#2	0.887(18)	2.14(2)	3.013(3)	167(4)
N(7)-H(7C)...O(13)#2	0.877(19)	2.10(2)	2.973(4)	172(4)
N(8)-H(8C)...O(6)#2	0.865(18)	2.17(2)	3.033(3)	172(4)
N(9)-H(9C)...O(3)	0.865(18)	2.08(2)	2.934(3)	172(4)
N(10)-H(10C)...O(12)#3	0.866(19)	2.06(2)	2.917(3)	171(4)
N(11)-H(11C)...O(2)	0.892(19)	1.96(2)	2.849(3)	173(4)
N(11)-H(11D)...O(8)#4	0.875(18)	2.07(2)	2.876(3)	153(4)
O(13)-H(13C)...O(3)	0.835(19)	1.94(2)	2.769(3)	174(5)

O(13)-H(13D)...O(10)#5	0.836(19)	1.95(2)	2.780(3)	172(4)
O(14)-H(14C)...O(13)	0.835(18)	2.01(2)	2.833(4)	170(4)
O(14)-H(14D)...O(6)#3	0.833(19)	2.12(2)	2.946(3)	175(5)

References

(1) Submeier, J. L.; Reilley, C. N. Nuclear Magnetic Resonance Studies of Protonation of Polyamine and Aminocarboxylate Compounds in Aqueous Solution. *Anal. Chem.* 1964, **36(9)**, 1698–1706.

(2) Baranyai, Z.; Botta, M.; Fekete, M.; Giovenzana, G. B.; Negri, R.; Tei, L.; Platas-Iglesias, C. Lower Ligand Denticity Leading to Improved Thermodynamic and Kinetic Stability of the Gd^{3+} Complex: The Strange Case of OBETA. *Chem. Eur. J.* 2012, **18(25)**, 7680–7685.

(3) Negri, R.; Baranyai, Z.; Tei, L.; Giovenzana, G. B.; Platas-Iglesias, C.; Bényei, A. C.; Bodnár, J.; Vágner, A.; Botta, M. Lower Denticity Leading to Higher Stability: Structural and Solution Studies of Ln(III)–OBETA Complexes. *Inorg. Chem.* 2014, **53(23)**, 12499–12511.

(4) Paulić, N.; Ivičić, N.; Jakopčić, K.; Simeon, Vl.; Weber, O. A. New Heterocyclic Analogues of EDTA. Synthesis and Physical Properties. *J. Inorg. Nucl. Chem.* 1977, **39(11)**, 2094–2095.

(5) Wanninen, E., *Acta Acad. Aboensis, Math. et Phys.* 1960, **21**, 17.

(6) Moeller, T.; Thompson, L. C. Observations on the Rare Earths—LXXV: The Stabilities of Diethylenetriaminepentaacetic Acid Chelates. *J. Inorg. Nucl. Chem.* 1962, **24(5)**, 499–510.

(7) Anderegg, G. Komplexone XXXVI. Reakinsenthalpie Und -Entropie Bei Der Bildung Der Metallkomplexe Der Höheren EDTA-Homologen. *Helv. Chim. Acta* 1964, **47(7)**, 1801–1814.

(8) Baranyai, Z.; Pálinkás, Z.; Uggeri, F.; Brücher, E. Equilibrium Studies on the Gd3+, Cu^{2+} and Zn^{2+} Complexes of BOPTA, DTPA and DTPA-BMA Ligands: Kinetics of Metal-Exchange Reactions of $[Gd(BOPTA)]^{2-}$. *Eur. J. Inorg. Chem.* 2010, **13**, 1948–1956.

(9) Wedeking, P.; Kumar, K.; Tweedle, M. F. Dissociation of Gadolinium Chelates in Mice: Relationship to Chemical Characteristics. *Magn. Reson. Imaging* 1992, **10(4)**, 641–648.

(10) Sarka, L.; Burai, L.; Brücher, E. The Rates of the Exchange Reactions between $[Gd(DTPA)]^{2-}$ and the Endogenous Ions Cu^{2+} and Zn^{2+}: A Kinetic Model for the Prediction of the In Vivo Stability of $[Gd(DTPA)]^{2-}$, Used as a Contrast Agent in Magnetic Resonance Imaging. *Chem. Eur. J.* 2000, **6(4)**, 719–724.

(11) Sarka, L.; Burai, L.; Király, R.; Zékány, L.; Brücher, E. Studies on the Kinetic Stabilities of the Gd^{3+} Complexes Formed with the N-Mono(Methylamide), N′-Mono(Methylamide) and N,N″-Bis(Methylamide) Derivatives of Diethylenetriamine-N,N,N′,N″,N″-Pentaacetic Acid. *J. Inorg. Biochem.* 2002, **91(1)**, 320–326.

(12) Pálinkás, Z.; Baranyai, Z.; Brücher, E.; Rózsa, B. Kinetics of the Exchange Reactions between $Gd(DTPA)^{2-}$, $Gd(BOPTA)^{2-}$, and Gd(DTPA-BMA) Complexes, Used As MRI Contrast Agents, and the Triethylenetetraamine-Hexaacetate Ligand. *Inorg. Chem.* 2011, **50(8)**, 3471–3478.

(13) Baranyai, Z.; Pálinkás, Z.; Uggeri, F.; Maiocchi, A.; Aime, S.; Brücher, E. Dissociation Kinetics of Open-Chain and Macrocyclic Gadolinium(III)-Aminopolycarboxylate Complexes Related to Magnetic Resonance Imaging: Catalytic Effect of Endogenous Ligands. *Chem. Eur. J.* 2012, **18(51)**, 16426–16435.

(14) Burai, L.; Hietapelto, V.; Király, R.; Tóth, É.; Brücher, E. Stability Constants and 1H Relaxation Effects of Ternary Complexes Formed between Gd-DTPA, Gd-DTPA-BMA, Gd-DOTA, and Gd-EDTA and Citrate, Phosphate, and Carbonate Ions. *Magn. Reson. Med.* 1997, **38(1)**, 146–150.

(15) Carnall, W. T.; Fields, P. R.; Rajnak, K. Electronic Energy Levels in the Trivalent Lanthanide Aquo Ions. I. Pr^{3+}, Nd^{3+}, Pm^{3+}, Sm^{3+}, Dy^{3+}, Ho^{3+}, Er^{3+}, and Tm^{3+}. *J. Chem. Phys.* 1968, **49(10)**, 4424–4442.

(16) Werts, M. H. V.; Jukes, R. T. F.; Verhoeven, J. W. The Emission Spectrum and the Radiative Lifetime of Eu^{3+} in Luminescent Lanthanide Complexes. *Phys. Chem. Chem. Phys.* 2002, **4(9)**, 1542–1548.

(17) Sillen, A.; Engelborghs, Y. The Correct Use of "Average" Fluorescence Parameters. *Photochem. Photobiol.* 1998, **67(5)**, 475–486.

(18) Agilent, CrysAlis PRO, Agilent Technologies Ltd, Yarnton, Oxfordshire, England, 2019.

(19) Sheldrick, G. M. SHELXT – Integrated Space-Group and Crystal-Structure Determination. *Acta Cryst. A* 2015, **71(1)**, 3–8.

(20) Sheldrick, G. M. Crystal Structure Refinement with SHELXL. *Acta Cryst. C* 2015, **71(1)**, 3–8.

(21) Farrugia, L. J. WinGX and ORTEP for Windows: An Update. *J. Appl. Cryst.* 2012, **45(4)**, 849–854.

(22) Macrae, C. F.; Bruno, I. J.; Chisholm, J. A.; Edgington, P. R.; McCabe, P.; Pidcock, E.; Rodriguez-Monge, L.; Taylor, R.; Streek, J. van de; Wood, P. A. Mercury CSD 2.0 – New Features for the Visualization and Investigation of Crystal Structures. *J. Appl. Cryst.* 2008, **41(2)**, 466–470.